Long-term performance of novel high-calcium one-part alkali-activated cement developed from thermally activated lime kiln dust

[*]Abdullah Kadhim[a, b], Monower Sadique [a], Rafal Al-Mufti [a], Khalid Hashim [a,b]

[a]Department of Civil Engineering, Liverpool John Moores University, Henry Cotton Building, Webster Street, Liverpool L3 2ET, UK.

[b]College of Engineering, University of Babylon, Babylon, Iraq.

[*]Corresponding author email address: a.m.kadhim@2017.ljmu.ac.uk, abdms93@gmail.com

Highlights

- One-part earth alkaline activated dry cementitious mixture was produced using thermally activated lime kiln dust (LKD) waste material as a source of CaO activator and metakaolin and natural pozzolan as a source of alumina-silicate
- The proportion of LKD and metakaolin in the ternary blend and thermal activation of LKD not only increased the reactivity but also induced higher degree of alkali-activation.
- Significant increase in the rate of strength development after 28 days of curing and continued until 180 days that reached 51 MPa for increased proportion of 950ºC calcined LKD and metakaolin in the blend was revealed.
- Considerable changes in mineralogy and amorphicity were evidently accredited to thermal treatment.

Abstract

The traditional activation approach for alkali-activated cement AAC has several problems resulting mainly from the hazardous and corrosiveness of the alkaline chemicals, such as (NaOH, Na_2SiO_3), which in turn impede the utilisation of AAC in the construction fields. In this study, A second generation of alkali activated binder was developed using Metakaolin (MK) and natural pozzolan material (NP) (as a source of alumina-silicate), these materials were activated using high-calcium lime kiln dust as solid activator to transform the alumina-silicate crystalline phases to cementitious hydrated products. This was achieved with the aid of heat treatment of materials at different temperatures. Raw materials and final AAC samples were characterised using analytical methods, such X-Ray powder diffraction (XRD), Thermogravimetric Analysis (TG-DTA), Fourier Transform Infrared Spectroscopy (FTIR) and Scanning Electron Microscope (SEM). Additionally, long-term compressive strength, chemical and microstructural performance were investigated. The transformation of raw materials from crystalline to amorphous phases happened due to the effect of the heat treatment and the formation of stratlingite products in the final AAC paste, which were evidenced using the mentioned characterisation methods. The findings of the present study proved that the compressive strength of the new binder reached 27 MPa and 51 MPa after 28 and 180 days of curing, respectively, ensuring a progressive as well as a higher degree of alkali-activation and disappearance of unreacted alkaline substances in the final AAC products.

Keywords

Alkali activated cement, heat treatment, Lime waste, XRD, TG-DTA, FTIR.

1. Introduction

The world production of the Ordinary Portland Cement OPC is significantly growing, where the estimated global production in 2018 was 4.1 billion metric tonnes [1]. The use of OPC in concrete construction is under serious evaluation because of the substantial challenges that are facing the method of production of conventional cement. Firstly, the high energy consumption through the whole process [2]. Secondly, a high quantity of carbon dioxide gas (CO_2) is released to the atmosphere during the production of cement [3]. To overcome these challenges, several investigations were commenced to develop other types of cements that are entirely free of OPC and based principally on supplementary materials. Mineral Products Association (MPA), in the UK, listed a number of novel low carbon (non-Portland) cements with low energy of production in their fact sheet [4]. One of these novel cements is Alkali Activated Cement AAC, which is a cementitious material formed as a result of an alkaline activation of amorphous or vitreous alumina-silicates. When mixed with alkaline activators (solid or liquids), in a chemical reaction called alkali-activation or alkalination, these materials set and harden, yielding a material with good binding properties [5,6]. There is a conventional two-part alkali activation, wherein a solid raw material is activated with alkaline chemical solution. This solution is categorised as extremely corrosive materials. From an operational viewpoint, they are difficult and expensive to handle, with significant occupational health and safety concerns. On the other hand, the activator solution provide the highest single contribution to the embodied carbon dioxide of AAC [7–9]. Until now, it cannot be said that AAC is based on user friendly and low carbon process, as the production of the chemical solutions releases large amounts of CO_2 to the environment [10].

Several efforts have been made to develop a second generation of geopolymers with one-part AAC that can be found under different terminologies in the literature, such as one-part alkali activated cement, self-activating cement or one-part alkali alumina-silicate hydraulic cement [11–13]. In one-part AAC, only a dry mixture is needed in addition to water. The dry mixture is prepared by mixing a solid alkali-activator with a solid alumina-silicate precursor, with or without an assisted activation approach [8,12].

Provis [14] defined the activators as any substance that represents an alkaline source that raises the pH of the reaction mixture and simplifies dissolution. This includes alkali cations (Na^+, K^+) or earth alkaline cations (Ca^{+2}, Mg^{+2}). A significant body of literature explored the synthesis of one-part AAC using alkaline commercial solid chemical activators, including sodium silicates (Na_2SiO_3) and sodium carbonates (Na_2CO_3). Realistic reports revealed that these chemicals are expensive and primarily contribute to the total cost of production of AAC [9,15–17]. Therefore, many synthetic chemicals do not represent a realistic commercial or environmental optimised solution for use as an activator [8].

Previous studies focused on the use of (CaO) and $Ca(OH)_2$ as potential alternative activators, as these activators are cheaper than (Na_2SiO_3) and (Na_2CO_3) [17,18]. These activators provide alkaline earth cations in place of alkali cations, which ease the creation of different binding phases,

when compared to blends of low calcium content [8,19]. Cabrera and Rojas [20] investigated the reaction kinetics of metakaolin-lime in water at 60ºC, using thermal analysis. The study confirmed the appearance of reaction products, mainly strätlingite (C_2ASH_8) and (C_4AH_{13}), as the reason for binder strength development. Kim et al. [17] used synthetic commercial CaO solid powder and ground granulated blast furnace slag (GGBS) (as the Si/Al source material) to produce non-cement binder . When compared to Ca $(OH)_2$, CaO activator was found to yield a higher mechanical strength, 53 MPa after 56 days, due to the production of more calcium silicate hydrate (C-S-H) than Ca $(OH)_2$. Nevertheless, when investigating the energy and ecological analysis of synthesising high purity chemical CaO powder, it was discovered that the synthesis process is complex, consuming high energy and it requires a high level of accuracy [21-22]. Different activation assisted methods were used in the production of a one-part AAC. For example, thermal activation (calcination) has been recently used as an assisted approach to improve the reactivity and the amorphicity of supplementary cementitious materials, such as natural pozzolans [11,23]. During the thermal treatment of undisturbed material, crystalline bonds are broken down and transformed to a glassy or amorphous phase, which results in a more reactive binder. When reviewing recent attempts directed to develop the one-part AAC, limited research projects have been devoted to investigate the long-term performance and properties of these materials, especially in the presence of unreactive alkaline substances. In fact, the latter must be precisely investigated as the excessive unreacted alkaline solution can be diffused to a concrete surface, and reacts with CO_2 in the air, forming efflorescence on the surface and degrading the appearance and strength of concrete [24].

Recently, Abdel-Gawwad et al.[25] carried out a study about one-part AAC comprised of GGBS and concrete waste treated by dry NaOH, with the addition of lead bearing sludge. The study assessed the compressive strength of hardened one-part AACs after 120 days, which was 44 MPa for a blend containing 65.9 wt. % GGBS, 15 wt. % lead bearing sludge, 34.10 wt. % concrete waste, 3.10 wt. % NaOH, 2 wt. % Na_2O, and water/powder ratio of 0.29. On the other hand, there is no study until now for evaluating the long-term strength of one-part AAC, activated by earth alkaline cations, such as CaO or MgO, embodied in the material.

The principal aim of this work is to develop of novel approach to produce a second-generation alkali-activated cement, that is completely free of commercial chemical activators. This was achieved by providing the earth alkaline source from lime kiln dust (LKD), which is primarily composed of reactive CaO. LKD is a by-product material of quick lime production process, which is usually disposed of in landfills worldwide. For instance, in the USA, it is estimated that about 2.5 million metric tonnes of high-calcium LKD is produced annually [26]. Thus, LKD must be reused to minimise its environmental impacts, and to meet the sustainability requirements. LKD is mainly composed of a CaO compound and high alkaline materials (high pH). Metakaolin, which is the crystallo-graphically disordered layered product of dehydroxylation of kaolinite (an alumina-silicate clay) [27], was combined with volcanic tuff or natural pozzolan(as an alumina silicate (Al/Si) source) to formulate the one-part dry AAC powder that just needs water to induce the alkali-activation process. Volcanic tuffs provide an extensive variety of reactivity, depending on

their degree of crystallinity and mineralogy. The proposed alumina-silicate precursors, undertake dissolution and precipitation processes when mixed with lime or CaO, yielding calcium alumina-silicate hydrate (C-A-S-H) [28]. Furthermore, the current research examines the long-term (after 180 days) mechanical and physico-chemical properties of the novel AAC cement, which helps to assess the sustained progression of alkali-activation in the absence of unreacted alkaline.

2. Materials and methods

2.1 Materials

The alumina-silicate source was produced by combining metakaolin (MK) and natural pozzolan (NP) from volcanic tuff material. LKD has been used as a source of alkaline material in the proposed blend. The elemental composition of raw materials was determined as they were received condition by using a Shimadzu EDX 720 and energy dispersive X-ray fluorescence (EDXRF) spectrometer. The key oxide elements and the physical properties of raw materials are listed in Table 1. Both MK and NP are composed of similar compositions of minerals, which could be considered as an ideal source of siliceous and aluminate materials, with minor quantities of CaO, Na_2O, K_2O and MgO in NP.LKD was mostly rich in CaO (about 80.1wt.%) with slight amounts of SiO_2 and Na_2O, and therefore it was considered as calcareous source. The specific surface area was determined by air permeability test (Blaine method) that is described in BS EN 196-6 [29]. It was found that MK and NP have surface area of 19.6 and 17.2 m^2/g, respectively, while LKD has 10.1 m^2/g, LKD has high alkalinity with pH of 12.3, which confirms its suitability to be alkaline activator. MK and NP have nearly the same density; 2.69 and 2.57 g/cm^3, respectively, while LKD has a density of 2.7 g/cm^3 as measured by Quantachrome gas expansion multi-pycnometer purged with helium gas.

Table 1. Chemical and physical properties of as received materials.

Chemical composition (Wt.%)	Raw materials		
	MK	**NP**	**LKD**
SiO_2	55	46.6	14.6
Al_2O_3	40	30.4	0.2
Fe_2O_3	1.4	3.8	0.1
CaO	0.15	4.5	80.1
Na_2O	0.4	3.9	1.8
K_2O	0.4	6	0.5
MgO	0.95	4.2	0.6
TiO_2	1.7	0.6	0.1
Physical Properties			
Specific surface area (Blaine) (m^2/g)	19.6	17.2	10.1
Density (g/cm^3)	2.69	2.57	2.7
pH	6	6	12.3

Particle size distribution (PSD), was determined using Beckman Coulter laser diffraction particle size analyser, as displayed in Fig. 1. It has been found that MK and NP have similar size distributions with D_{50} of 9.22 and 7.87µm, respectively. Conversely, LKD was found to be coarser, with a D_{50} of 15.94µm. This particle size range of raw materials has a high positive effect on alkali activation. Rashad et al. [30], reported that MK with grain size less than 32 µm yields a workable mix with higher compressive strength.

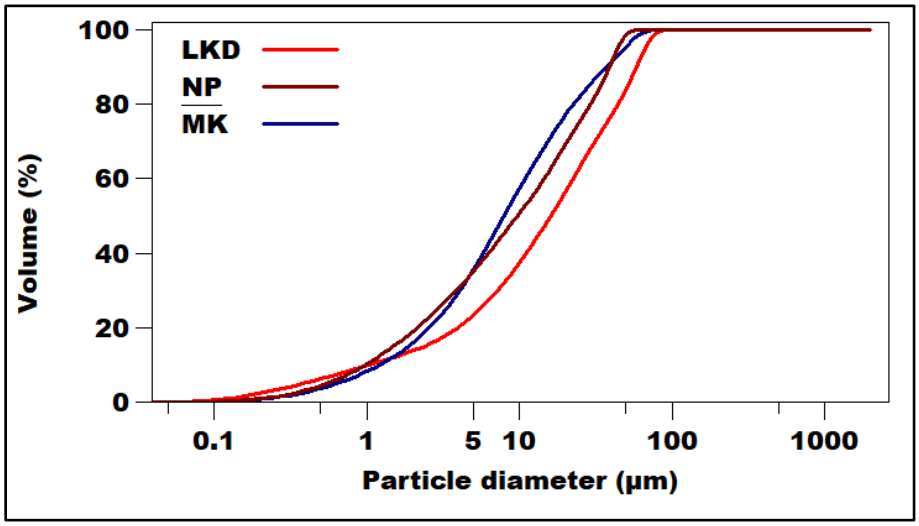

Figure 1. Particle size distribution (PSD) of starting materials.

2.2 Testing methods

The set of experimental tests that have been conducted in this study comprises of fresh properties indexed by the setting time, mechanical properties indexed by the compressive strength, thermal analysis presented by thermogarvemetric analysis (TGA) and microstructural analysis introduced by x-ray diffraction (XRD), Scanning Electron Microscope (SEM) and Fourier transform infrared spectroscopy (FT-IR).

2.2.1 Setting time

The standard consistency and setting time of the developed one-part AAC binder were investigated according to British standard 196-3 [31].

2.2.2 Compressive strength

The compressive strength of mortar prisms, was used as a function for evaluating the mechanical properties of specimens and was measured according to the British standard 196-1 [32]. The test was carried out using a Control Automax 5 compression tester, with a load rate of 0.4 MPa/sec.

2.2.3 Thermal analysis (TGA)

Thermal analysis used in this investigation, consisted of Thermogravimetric analysis (TG), which is usually used to determine weight loss of the samples that subjected to thermal events. However, this technique does not detect phase change, such as “melting”; thus, differential thermal analysis (DTA) is employed, which is the first derivative of the weight loss curve. DTA indicates phase changes as endothermic and exothermic peaks [33]. Therefore, it is donated as TG-DTA technique. The tests were completed using the Perkin Elmer TGA Q50 V20.13 Build 39. The thermal performance of materials was investigated by TG-DTA, with a heating range 20-900 ^{o}C and a heating rate of 10 ^{o}C/min. In this study, TG-DTA investigations were performed on raw materials to assess their thermal behaviours during individual calcination.

2.2.4 Microstructural analysis

The microstructural and morphological analyses were carried out on the raw materials before and after thermal treatment. Additionally, the selected pastes of AAC, with the highest strength after they have been hydrated and hardened, were finely ground, dried, and have gone through XRD, SEM and FT-IR analysis after 28, 90 and 180 days of curing. The XRD test was carried out using a Rigaku mini-flex diffractometer (mini-flex goniometer), with CuK X-ray radiation (30 kV voltage and 15mA current at scanning speed of 2.0 deg./min in continuous scan mode) and scanning range (2θ) of 5–60°. Scanning Electron Microscope (SEM) morphological analysis and observations were conducted using an Oxford Inca x-act detector (45nA prob current and 100 sec counting time) and a FEI Company SEM model Inspect S (20kV accelerating voltage). Fourier transform infrared spectroscopy (FT-IR) analysis was carried out using a Perkin-Elmer Spectrum BX series Fourier transform infrared spectrometer (FT-IR), equipped with a Miracle ATR accessory (Specac, UK). The spectrum of the sample was recorded using accumulating 16 scans at 4 cm^{-1} resolution and wavelength between (550 cm^{-1} and 2000 cm^{-1}).

2.3 Characterisation of raw materials

The powder (XRD), (SEM) and (FT-IR) analyses of undisturbed materials are illustrated in Figs. 2 to 4. From the X-Ray diffractions of MK, Fig. 2, it is observable that MK comprises many crystalline phases and is primarily composed of quartz (SiO_2) and Mullite ($Al_6Si_2O_{13}$), in major crystalline peaks. Illite (K, H_3O) $(Al,Mg,Fe)_2(Si,Al)_4O_{10}[(OH)_2,(H_2O)]$ and anatas (TiO_2) compounds in minor peaks. The highest quartz peak occurred at (2θ) 26.73º. Diffractogram patterns of NP, which have closely crystalline peaks of quartz peak and feldspars, such as anorthite ($CaAl_2Si_2O_8$) and clinoptilolite (KNa_2Ca_2 $(SiO_{29}Al_7)$ O_{72} $24H_2O$). Additionally, edenite (Ca_2NaMg_5 $(AlSi_7)$ O_{22} $(OH)_2$) was present in NP diffractions with high quantities. Diffractions of LKD, showed one recognised crystalline peak of calcite ($CaCO_3$) with a higher intensity. Smaller peaks exist in the forms of mullite. The presence of such compounds increases alkalinity activity in LKD; these compounds are similar to the content of commercial activator water glass (Na_2SiO_3).

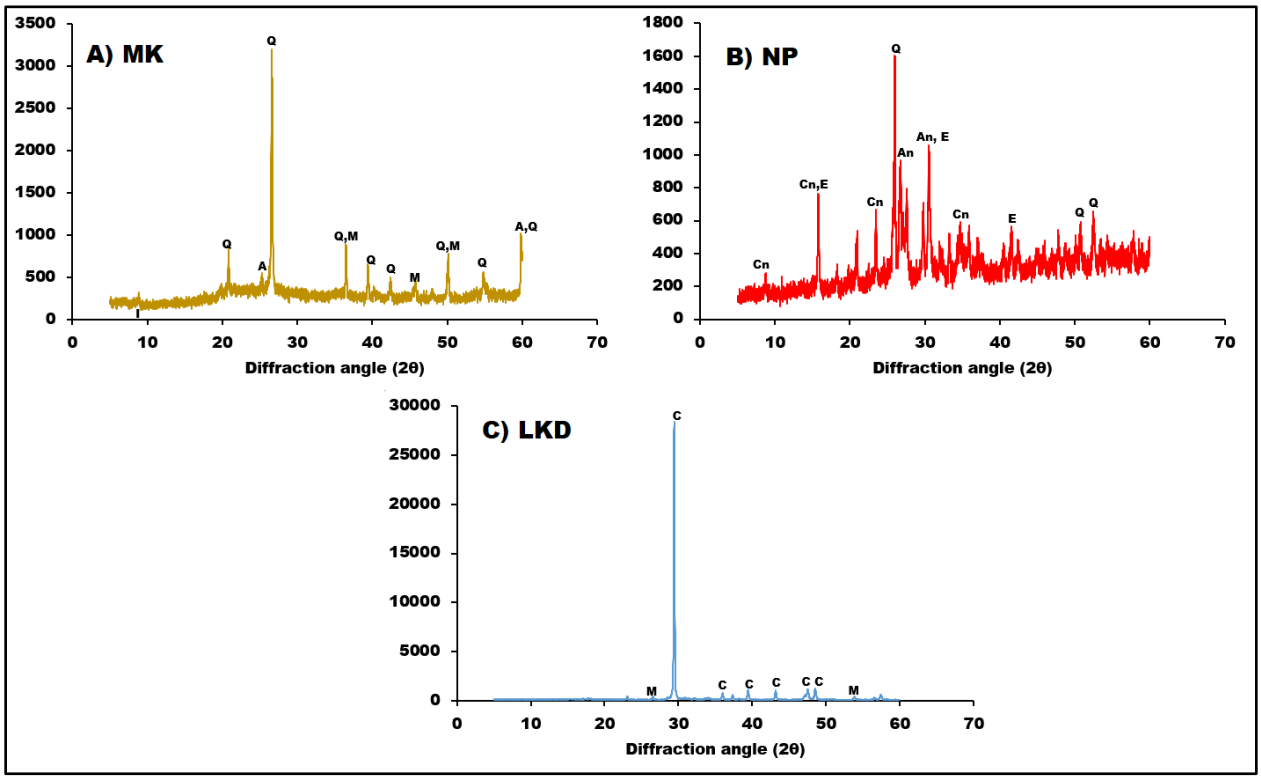

Figure 2. Powder XRD-patterns of initial materials

Q: Quartz, M: Mullite, A: Anatas, I: Illite, Cn: Clinoptilolite, An: Anorthite, E: Edenite, C: Calcite.

SEM images illustrate the particles of original materials, as shown in Fig.3. MK seems to have fine and lamellar particles with random non-uniform shapes. Particles of LKD look coarser and have less surface area with flaky shapes. The raw NP particles, as shown in the SEM image, are irregular in shape and size.

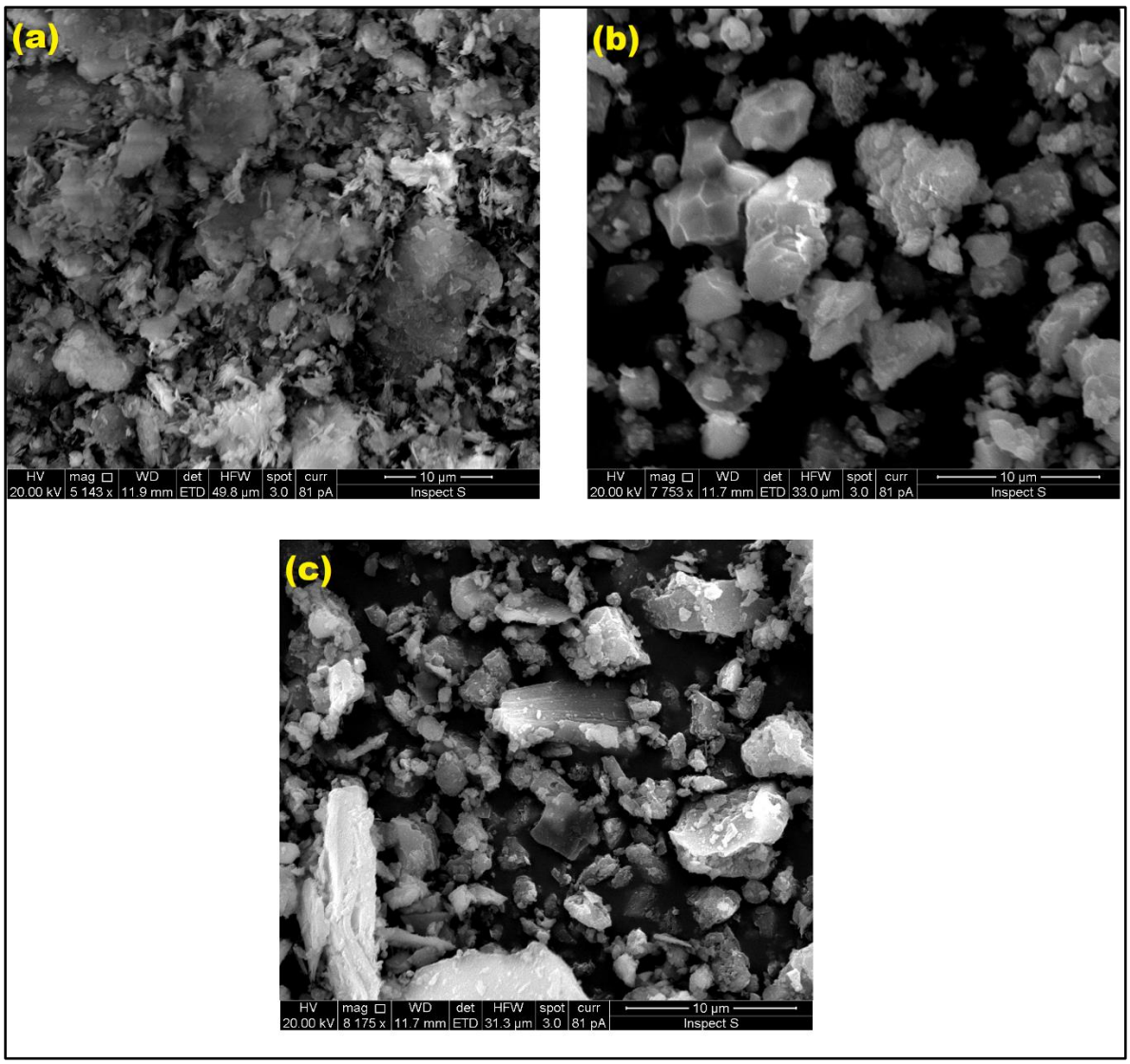

Figure 3. SEM micrographs of undisturbed materials a) MK, b) LKD and c) NP.

Fig. 4 shows the results of the FT-IR measurements of raw MK and NP, which indicate that the highest absorption band of these raw materials are 1046 and 996cm^{-1}, respectively These values are attributed to the strong bands of Si–O–Al and tetrahedral Si–O–Si of bridging oxygen (BO) atoms of the original alumina-silicate framework [34]. The characteristic peaks appearing at 794cm^{-1} and 724cm^{-1}, are ascribed to the stretching vibration Si–O and stretching Al 6-coordinated geometry (AL, Mg)–O–OH [35]. Both absorptions Si–O–Si and Si–O, are supporting the presence of quartz, while Si–O–Al is supporting the presence of kaolinite [35,36]. These peaks are related to the alumina-silicate prevalence phases in both MK and NP. The strong presence of calcite ($CaCO_3$), presented by the C–O bond, was evidently presented by the bands at 1402, 872 and 712cm^{-1} [37]. The presence of these bands is accredited to the tendency of CaO to react naturally with CO_2 in the atmosphere.

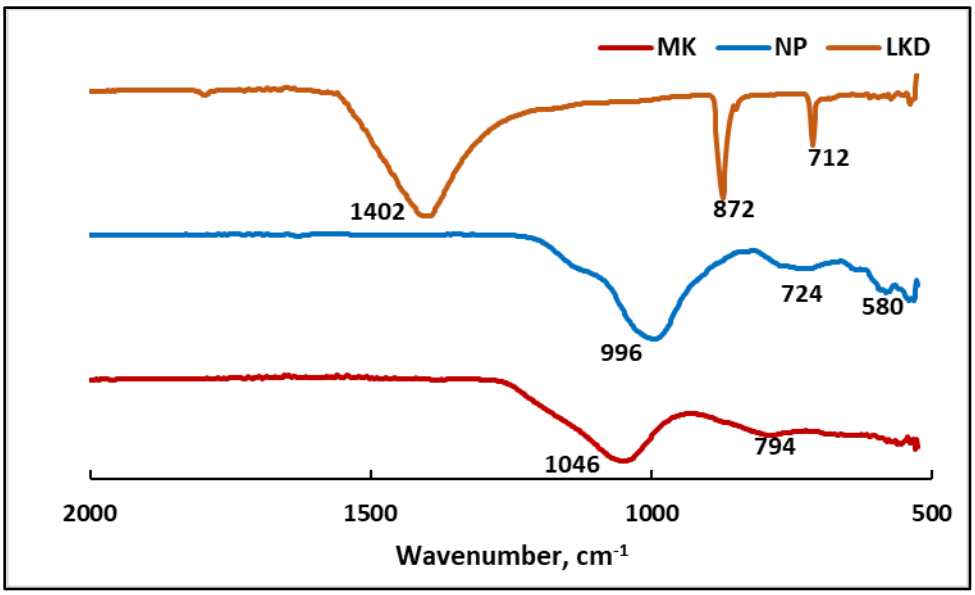

Figure 4. FTIR-spectra of as received materials

2.4 One-part AAC cement preparation

2.4.1 Heat treatment mechanism

Thermal treatment or calcination, means heating the substance to high temperature (500-2000 ^{o}C) within a controlled atmosphere, in order to increase their reactivity by changing their mineralogy [23]. Thermal treatment is used as one of the assisting activation methods to produce one-part AAC cement. Most of the materials, which are clayey in origin, require calcination in order to be reactive. For instance, metakaolin ($Al_2Si_2O_7$) is originally synthesised from the calcination of kaolin clay (Al_2SiO_5 $(OH)_4$) [38] at a temperature of 750 ^{o}C that used in current study. During the calcination process, dehydroxylation is carried out, leading to the loss of the long-range order of alumina and silica layers and conversion of the powder to an amorphous form so that when they react with calcium hydroxide and water, they undergo a pozzolanic reaction to form hydration products responsible of improving the strength and durability [39]. Another change is that the alumina transforms from the octahedral coordination to tetrahedral coordination, due to calcination [40]. On the other hand, recent studies demonstrated that the transformation of metakaolin into spinal structure of Si-containing γ-Al_2O_3 and amorphous silica does not occur in temperatures less than 920 ^{o}C [41,42]. Therefore, in order to enhance the reactivity of calcined kaolins so that it can be used as a pozzolanic cement products, a proper thermal treatment for metakaolin (for structure disorder) is essential [41,43].

On another aspect, significant amounts of lime kiln dust (LKD) are produced, during the calcination process of limestone, and collected from dust control systems. LKD usually contains variable amounts of free/available CaO/and un-calcined calcium carbonates, and less amounts of impurities, such as MgO, derived from the limestone [44] and dumped in waste landfills due to its high amounts of impurities which is environmentally not favourable alternative. Earlier

investigation by Strydom et al.[45] to determine the reactivity and phase changes of precipitator dust from lime kilns upon heating to 500 ^{o}C and 1000 ^{o}C, has observed slight reduction in the intensity of the recognised calcite at temperature 500 ^{o}C and complete disappearance of calcite and transformation to CaO at 1000 ^{o}C, which makes LKD as hydraulic materials to participate in hydration reaction. Furthermore, NP, which is a natural pozzolan material, is considered as a good source of silicate and aluminate, but in a poor reactivity state it must be treated by various methods, such as chemically or thermally, to enhance its reactivity which was repeatedly confirmed previously by many literature [46–48].

Thermal activation was performed, in this study, for the candidate materials individually to increase their reactivity. Subsequently, mixing each calcined material with the other two non-calcined precursors, according to the blending concept (Si/Al+alkaline), was carried out to synthesise a dry hydraulic cement, as illustrated in Fig. 5. Thermal treatment was conducted in a muffle furnace with a ramping temperature of 20 ^{0}C/min for 2 hours. Two foundry cylindrical silicon carbide graphite crucibles (500ml) and two alumina cylindrical crucibles (175ml), were used during calcination process. The relevant literature demonstrated that crystallinity and reactivity of most materials rich in alumina-silicate content can increase with temperatures up to 950-1000^{o}C, but after this temperature range, their reactivity can be decreased [49,50]. In this study, activation at temperatures of 450^{o}C and 950°C have been investigated to evaluate and compare the phase transitions. Activation at 450^{o}C temperature at mid-range between 0 and 950^{o}C to evaluate and compare the phase's transitions aimed for saving energy. It is noteworthy to mention that the choice of activation temperatures was based on TGA and XRD analysis (discussed later), which revealed that most phase transitions occur at these levels.

Additionally, it is noteworthy that during thermal activation process; some of the material colours have been changed in both stages of temperatures, as displayed in Fig 5. The colour of MK was becoming whiter, with the increase of temperature, while, the colour of NP has shown considerable change from greyish to brown, as the temperature rose. The colour transformation of NP attributed to the increment of anorthite mineral that has been observed clearly in XRD patterns, which turns to be brown in nature [51]. LKD originally white but turned into light grey at 950^{o}C.

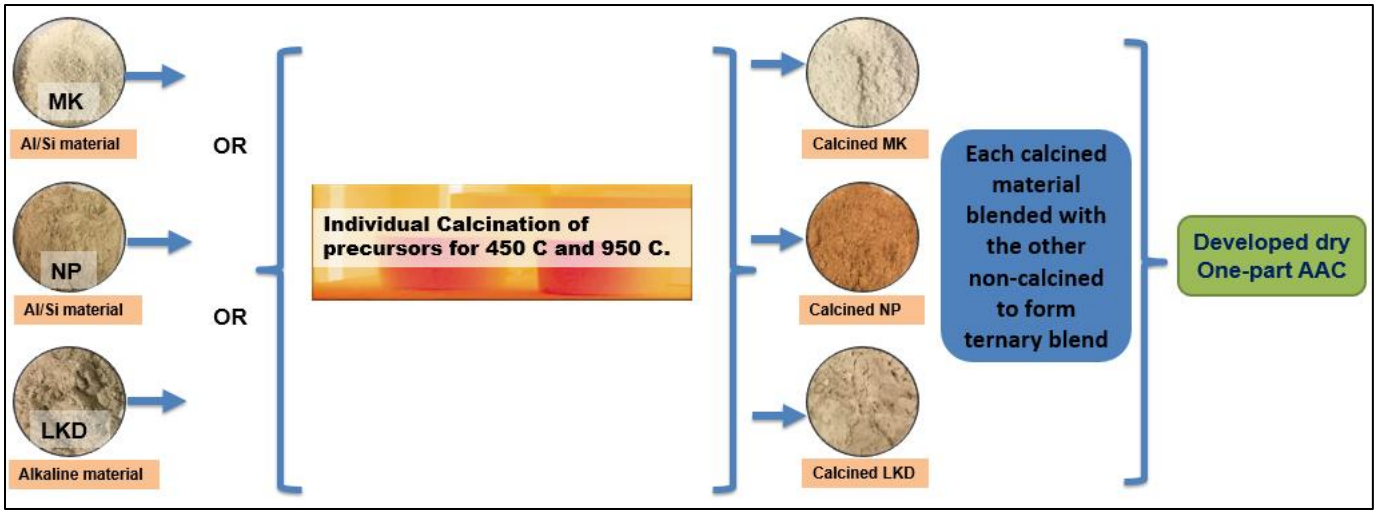

Figure 5. Preparation steps of one-part alkali activated cement.

2.4.2 Preparation of one-part AAC mortars

Mortars were mixed with kiln dried sand, with a specific gravity of 2.62, with sand to binder ratio of 1:2. The particle size distribution of the used sand is shown in Fig. 6. The mixing process was conducted according to the requirements of British standard 196-1 [32]. Initially, 0.55 water/binder ratio was chosen, but it was found that the mortars were extremely flowable, therefore; it was reduced to 0.45 for all the mortars, where appropriate consistency was achieved at this stage.

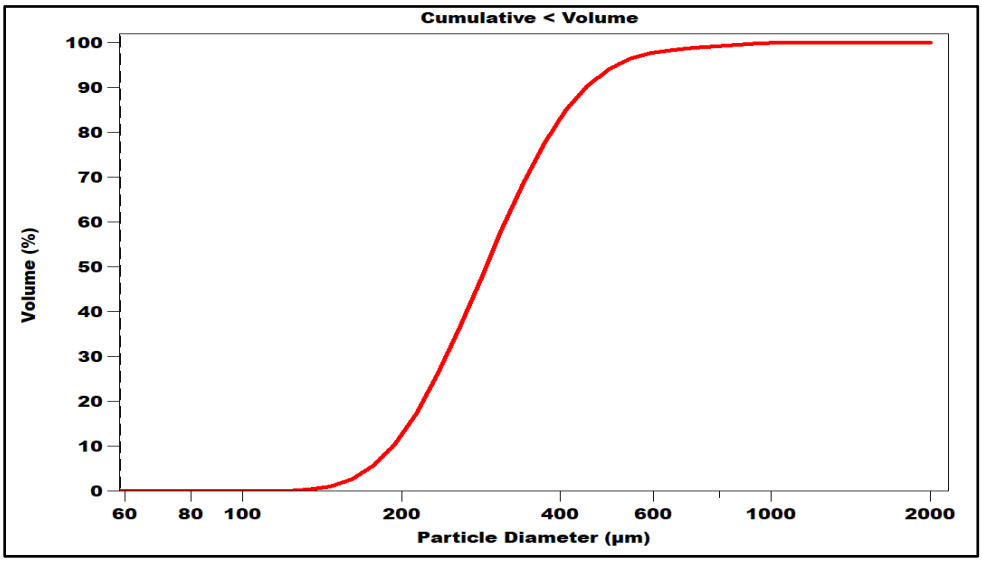

Figure 6 Particle Size Distribution of the sand used for mortar.

Mortars were mixed, using a Hobart 5L countertop Mixer N50, and poured in steel prism moulds (40mm x 40mm x 160mm). Mortars were prepared using ternary blended binder with proportions, as shown in Table 2. These mix proportions, in the ternary blends, were achieved after several initial trials, as the ternary blended with only non-calcined constituent, showed no cementing property after 28 days of curing.

Table 2 Mixing proportions of ternary blends used for preparing mortar specimen.

Mix ID	Binder contents	Calcination temperature (°C)	Calcined constituent
AAC1	40%MK 40%LKD 20%NP	950	NP
AAC2	40%MK 40%LKD 20%NP	950	MK
AAC3	40%MK 40%LKD 20%NP	950	LKD
AAC4	40%MK 40%LKD 20%NP	950	NP, MK, LKD
AAC5	35%MK 35%LKD 30%NP	950	NP
AAC6	35%MK 35%LKD 30%NP	950	MK
AAC7	35%MK 35%LKD 30%NP	950	LKD
AAC8	35%MK 35%LKD 30%NP	950	NP, MK, LKD
AAC9	35%MK 35%LKD 30%NP	450	NP
AAC10	35%MK 35%LKD 30%NP	450	MK
AAC11	35%MK 35%LKD 30%NP	450	LKD
AAC12	35%MK 35%LKD 30%NP	450	NP, MK, LKD

The mortars were cured in a hot water curing regime, to enhance the reactivity and the alkali-activation rate of the mortars and to avoid potential problems, such as efflorescence and micro cracking, which can lead to a reduction in the compressive strength [52]. Curing temperature was fixed to 50 °C for the first 7 days, and then cured in normal water (20 °C) for the desired period, as suggested by Perera et al. [53] and Singh et al. [54].

3. Results and discussion

3.1 XRD analysis after heat treatment

The powder diffraction of calcined materials has been presented in Fig. 7. Diffractograms of MK revealed a significant reduction and disappearance of peaks, such as mullite and illite, after both levels of calcination indicating semi-transformation of material to an amorphous phase. While peak of quartz has shown no change on both calcination level, XRD spectrums of calcined NP at both levels, indicated a huge transformation of crystalline phases to amorphous phases through the loss of quartz and clinoptilolite, in a range of 2θ from 30 ° to 60°. It can be noticed, that crystalline quartz, which peaked at 2θ = 26°, has disappeared entirely when NP calcined to 450°C and 950°C, introducing strong evidence of the increment of amorphicity. This was confirmed by the formulation of a broad amorphous hump of anorthite existed at 2θ = 26.7° and 2θ = 27.8° at 950°C patterns. Remarkably, this intense calcite peak in LKD was reduced markedly when calcined to 450°C and completely disappeared in calcination at 950 °C which could indicate the total decomposition of calcite $CaCO_3$ to lime CaO and introduced as new peaks at 2θ = 37° and 54°.

The appearance of new diffraction patterns of calcined LKD at 950°C, indicated the formulation of new compounds, but it was composed of the same elements as untreated LKD (CaO, SiO_2 and Al_2O_3), in the form of periclase cementitious minerals, di-calcium silicate C_2S (2CaO.SiO2) and gehlenite ($Ca_2Al(Al\ Si)O_7$) [45]. This would suggest that mullite ($3A1_2O_3.2SiO_2$) exist in raw LKD has decomposed and reacted with CaO to formulate these new phases [45]. The complete disappearance of the intense crystalline CaO after 950°C calcination, which indicated that calcination had caused a large combination of lime CaO with the compounds of SiO_2 and Al_2O_3, to form the above hydraulic minerals.

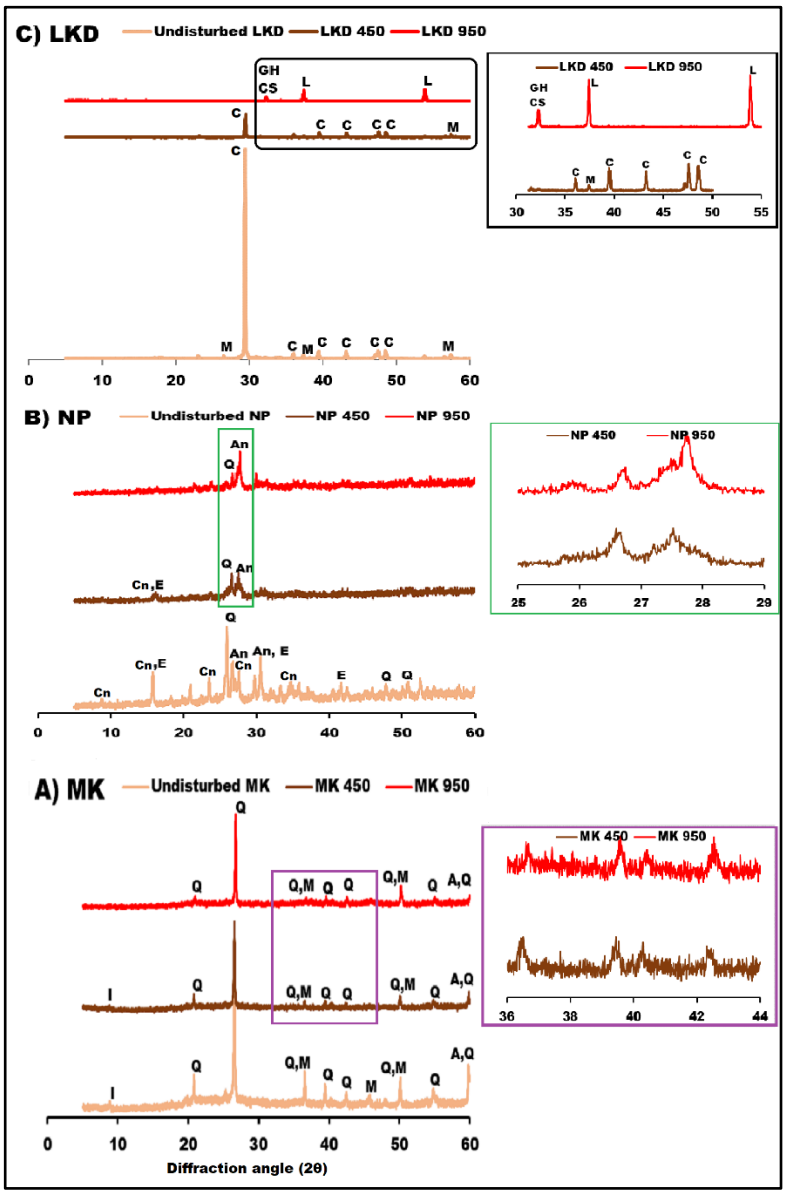

Figure 7. Powder XRD patterns of materials after thermal activation, A) MK, B) NP, and C) LKD.

Q: Quartz, M: Mullite, A: Anatas, I: Illite, Cn: Clinoptilolite, An: Anorthite, E: Edenite, L: Lime, C: Calcite, CS: dicalcium-silicate, GH: gehlenite

3.2 FT-IR analysis after heat treatment

The FT-IR spectrums of thermally treated materials are illustrated in Fig. 8. The alumina-silicate bands Si-O-Si and Si-O-Al have become higher from 1046 cm^{-1}, in untreated MK, to 1058 cm^{-1} at 450 ^{o}C and 1078 cm^{-1} at 950 ^{o}C. This is while the opposite to this tendency took place with the spectra of NP. This kind of shifting and enhancement of broadness of these bands, leads to the transformation of crystalline phases to an amorphous structure and high deformation in the lengths and angles of Si–O–Al and Si–O–Si bonds [25]. This transformation is satisfied by the increment of non-bridging oxygen atoms due to thermal treatment [55]. A considerable reduction and width increment of the intensity of C-O bond during the treatment at 950^{o}C, indicates the transformation of the crystalline phase into the glassy phase and interprets the increment of CaO amounts released from $CaCO_3$ [56,57].

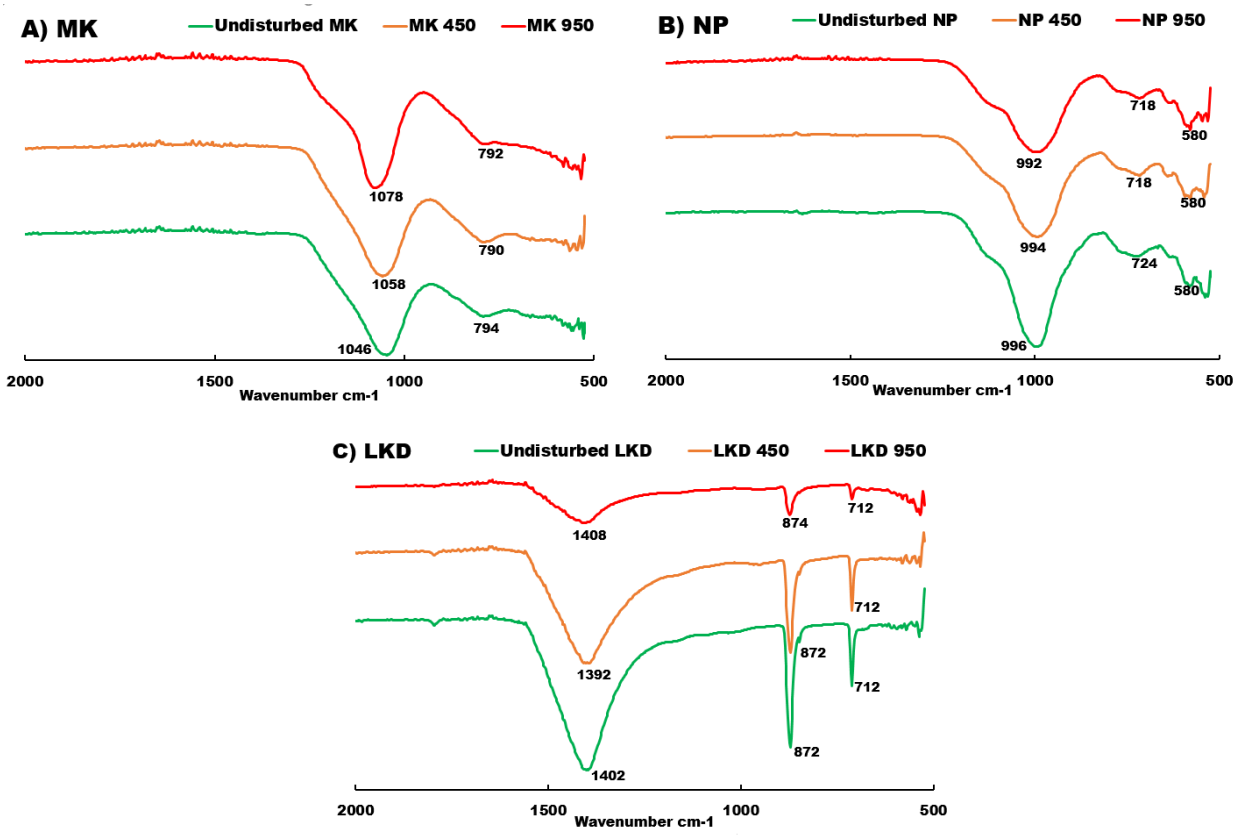

Figure 8. FTIR spectra of materials after thermal activation.

3.3 Thermogravimetric Analysis (TG-DTA) after heat treatment

Fig. 9 (A) exhibits the thermal performance of NP investigated by TG-DTA, when calcined to 900^{o}C. As can be seen, some mass-loss phases are present in its patterns caused by endothermic and exothermic reactions. The Thermogravimetric (TG) patterns of NP mass-loss from room temperature to 900^{o}C is approximately 7% of total weight, which might be attributed to the loss of

chemically and physically adsorbed water and breakdown of crystal phases, which was evidenced by XRD analysis. The loss of weight can be divided into three stages. The loss in temperature range of 20-320^{o}C is due to the evaporation of adsorbed water. The loss in the range of 320 – 620^{o}C, is because of calcining amounts of impurities and contaminants. While loss in the range 620 - 900^{o}C is due to decomposition of unburnt carbons [58,59]. As for the DTA curve, there was endothermic convexity at 119^{o}C, which relates to the evaporation of water followed by exothermic concavity at 250^{o}C. The TG curve of MK has shown a very small weight change within 2% of the total weight, with a reasonably straight DTA curve, as shown in Fig. 9B. The TG patterns of LKD, revealed that it has not lost any weight until 350^{o}C; when there was only a slight weight loss until 620^{o}C, when the weight changed dramatically with a 35 % loss of original weight and an exothermic sharp peak of the DTA curve, which is shown clearly in Fig. 9C. This loss is markedly attributed to the transformation and loss of the CaO crystalline intense peak, which was further evidenced by the XRD analysis of 950^{o}C calcination, when this peak disappeared from the diffraction pattern.

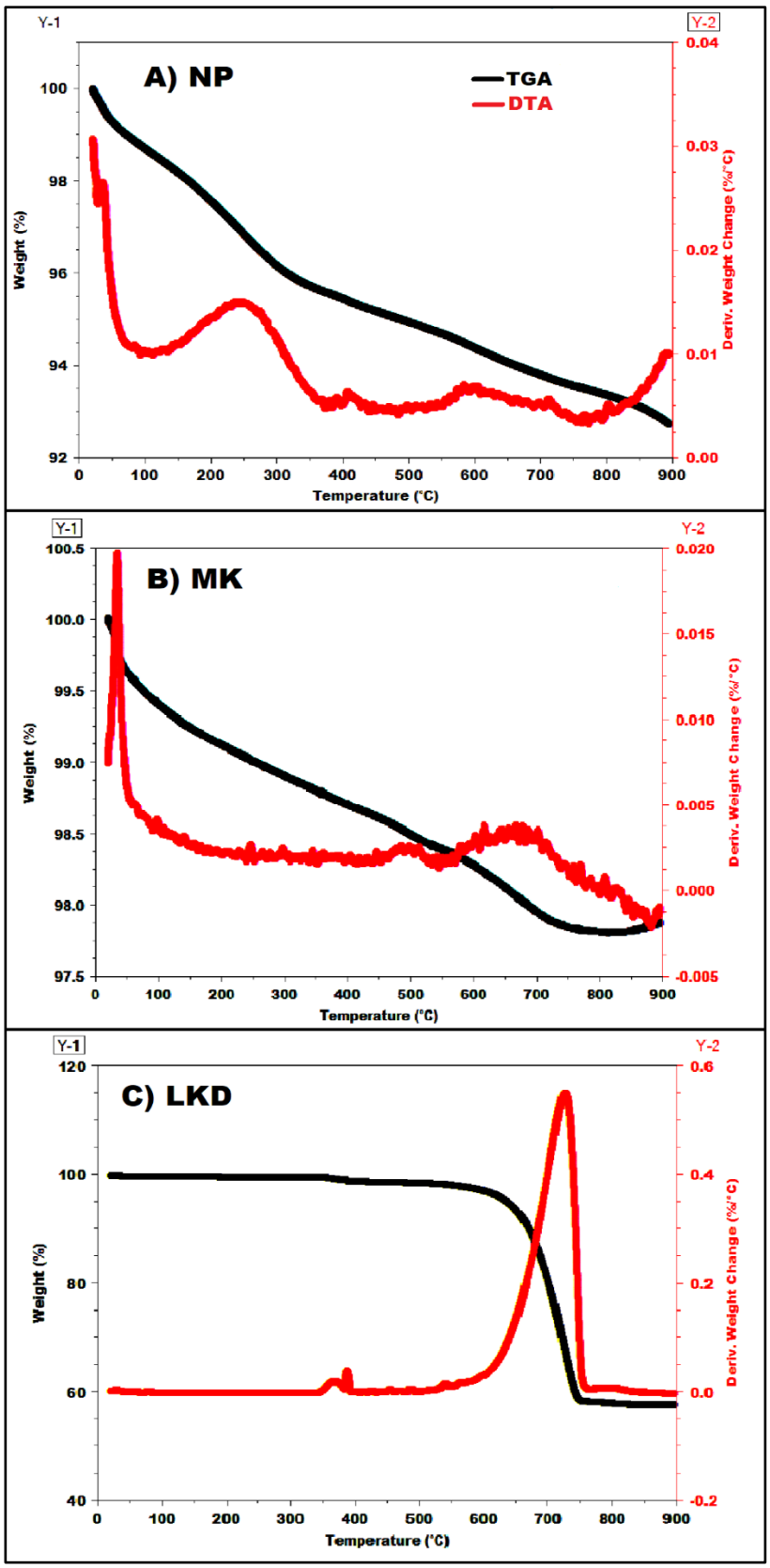

392

393 *Figure 9. TG-DTA analysis of initial materials, A) NP, B) MK, and C) LKD*

3.4 Influence on compressive strength after heat treatment and blending.

One-part mortar samples were prepared and cured using the mix proportion, with two levels of thermally activated materials as stated in table 2, and their resulting compressive strengths are displayed in Figs. 10 and 11. The blend containing 950ºC calcined LKD (AAC3), has shown a compressive strength of 24.54 MPa after 28 days. The regular growth in strength of up-to 28 days for this blend, indicates the progressive alkali-activation that attributes to the calcination of LKD with the presence of sufficient amounts of reactive silicate and calcium oxide from the NP. A considerable amount of strength was developed within the blends, containing calcined materials individually and collectively, which showed no cementitious properties prior to thermal treatment. Calcination at 950ºC, clearly contributed to a huge variation in LKD mineralogy and substantial reduction in its crystallinity, which was observed in the XRD patterns. In order to optimise the strength, these mortar mixes were repeated with same procedures, but with increased proportion of NP (35% MK, 35% LKD, and 30% NP). The increment of the NP was due to the suitable composition of NP, which contains a various range of alkaline elements including CaO, Na_2O and K_2O, as shown in XRF results. Noticeably, the highest compressive strength was achieved at this stage with 27.3 MPa in 28 days for the blend that contains 950ºC calcined LKD (AAC7), as shown in Fig. 10. The increment of NP content by 10% within the blends, resulted more growth of C-A-S-H products. The addition of more NP contributed to extra dissolution of quartz silicate, caused by CaO and Na_2O that exists in the calcined LKD and NP, yielding high binding properties. Therefore, a higher transformation to vitreous mineralogy led to a higher strength of AAC7. Moreover, the reduced strength for AAC4 and AAC8, when all three components were calcined, indicated less dissolution of Si/Al compounds from MK and NP (at both composition), which means that less activation was caused by the LKD.

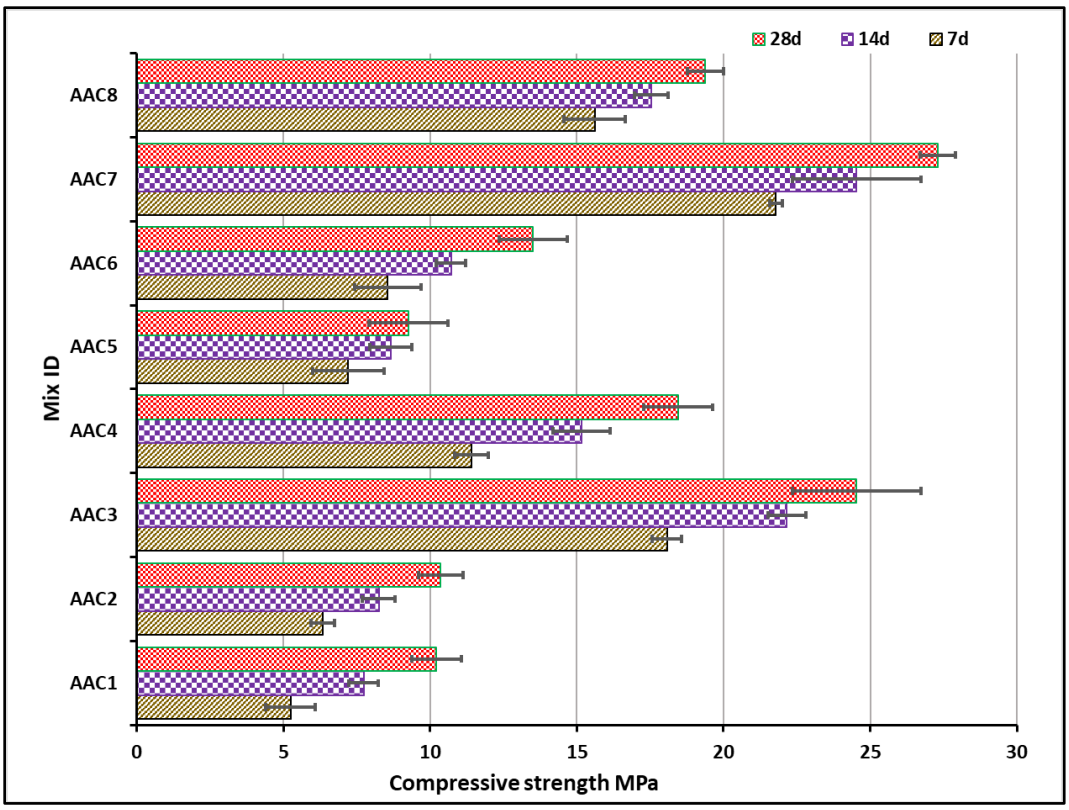

Figure 10. Compressive strength of blends with 950 °C calcined materials.

The TG-DTA curves have shown that the weight loss of the individual constituent of the ternary blend, starts at the temperatures in the range 350-500°C. This was evidenced by XRD patterns, where raw materials after 450 °C treatment have displayed a considerable change in their diffraction. Therefore, the ternary blends of 35% MK, 35% LKD and 30% NP were formulated after calcination of 450°C. The resulting compressive strength offered by the ternary blends after 450°C thermal activation, has been shown in Fig. 11. A similar trend of higher strength in the case of calcining LKD individually at 450 °C, was evident in AAC11 with 23.4 MPa at 28 days. Although both early and longer-term strengths were higher in the case of 950°C treatment, no remarkable strength generation was observed compared to a lower temperature (450°C). This similar development of strength is ascribed to mineralogical and chemical changes that were noticed in both XRD and TG-DTA results, which indicated that most of diffraction patterns were starting to transform around and after 450°C.

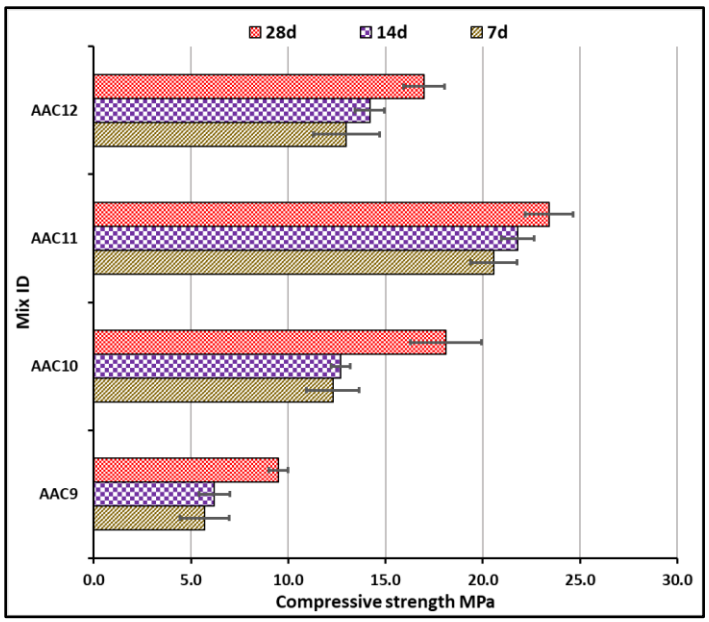

Figure 11. Compressive strength of blends with 450 ^{o}C calcined materials.

3.4.1 Long-term compressive strength for optimal blends

The compressive strength after 90 and 180 days of curing was investigated for the blends, which showed a higher alkali-activation rate in the case of calcined LKD at both level of calcination and mix proportion (AAC3, AAC7 and AAC11), as presented in Fig. 12. Although AAC3 has a lower compressive strength than AAC7 until 28 days of curing, it showed significant increase in rate of strength development just after 28 days and continued till 180 days. The higher rate of strength growth has been witnessed at the later age of 180 days which has shown increment of strength to reach 51 MPa for blend AAC3 and 45 MPa for AAC7 with increment of about 11% and 18% at age of 90 days of both mixes respectively; indicating that there was a high degree of alkali-activation within the system until 180 days, without showing any marks of efflorescence. The higher degree of polymerisation within AAC3 compared to AAC7 was due to the formulation of balanced alumina silicate and alkaline materials, which was achieved through reducing 10% of NP and adjusting the others accordingly. This is was due to the higher CaO contained in AAC3 that promoted formulation of further amounts of geopolymeric products and more stable microstructure. This can be justified that calcium cations (Ca^{+2}) might be bonded in the geopolymeric gel that results in charge balance by replacing cations within the geopolymer [60]. The chemical mechanism of combining calcium cations in geopolymeric gel is illustrated by the following reactions [61,62]:

$$\equiv Si\text{-}O^{-} + Ca^{2+} \rightarrow \equiv Si\text{-}O^{-}Ca^{+} + H_2O$$

$$\equiv Si\text{-}O^{-}Ca^{+} + O^{-}Al + H_2O \rightarrow [\equiv Si\text{-}O\text{-}Ca\text{-}O\text{-}Al\equiv]$$

$$\rightarrow \equiv Si\text{-}O\text{-}Al\equiv + Ca^{2+} + 2OH^{-}.$$

Contrariwise, sample containing calcined LKD at 450ºC (AAC11), has promoted a slight deterioration in strength immediately after 28 days and continued until 180 days. This signifies the inhibition of the alkali-activation reaction after 28 days in this blend. While the combined procedures of impurities disappearance that were contained in the chemical composition of LKD as a by-product material and the mineralogical changes after thermal treatment have strongly introduced the fact that reactivity of LKD has increased just after thermal treatment. To confirm this fact, this was investigated by preparing a mortar sample similar to AAC7 but without the application of thermal treatment to LKD, as this sample has the optimal strength at the age of 28 days, 51% lower compressive strength (18 MPa) after 28 days was achieved from that blend, that comprised un-calcined LKD, and decreased to 16 MPa at age of 180 days.

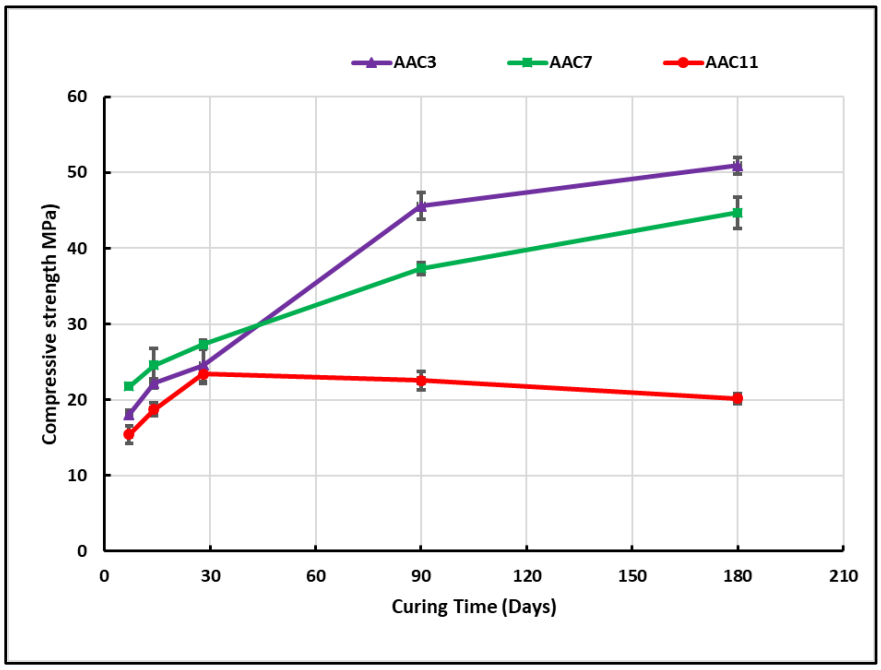

Figure 12 : Long-term strengths of one-part blends containing activated LKD at 450 ºC and 950 ºC.

3.5 Setting time

Fig. 13 shows the initial IS and final FS setting time of the optimum blends AAC3, AAC7 and AAC11. It can be observed that the setting times for blends are fluctuating between 61-87 min for the initial setting time and between 78-110 minutes for final setting time. It can also be noticed in Fig.13 that nearly parallel IS and FS for blends AAC3 and AAC7, indicating that slower alkali activation is due to the higher content of calcined LKD (40 Wt.% and 35 Wt.%), which acts here as a key activation agent. Higher amounts of alkaline cations of Ca^{+2} from LKD in the system is leading to the formation of extra $Ca(OH)_2$ that causes more breaking and dissolving of Si and Al chains that accelerates the alkali-activation reaction, and consequently increases the setting time [63]. However, lower IS and FS were observed in AAC11, as shorter levels of reactions occurred due to the low reactive LKD and, therefore, lower alkali activation. The effect of the alkaline cations, from the activator (LKD), was clearly seen on the setting time. The result was evident, as

the alkaline part became more reactive, as there was more dissolution, leading to longer setting time.

In terms of application and use of AAC, a higher setting time is a significant parameter for transporting far distances, storage and a shorter setting time, which is important for quick repairs of damaged surfaces [63]. The current results of IS and FS are in a good agreement with the results of past studies. For example, Luukkonen et al. [8] revealed in their review that IS and FS of developed one-part AAC in past attempts were from 23-150 and 69-230 minutes, respectively. Additionally, the obtained results of initial setting time in this study are in agreement with initial setting times for cement types in British standards 197-1 [64]. Furthermore, setting times can be easily increased if needed in some applications with the aid of setting retardant agents such as lignosulfonate which was proven as a suitable retarder for one-part AAC in past studies [65].

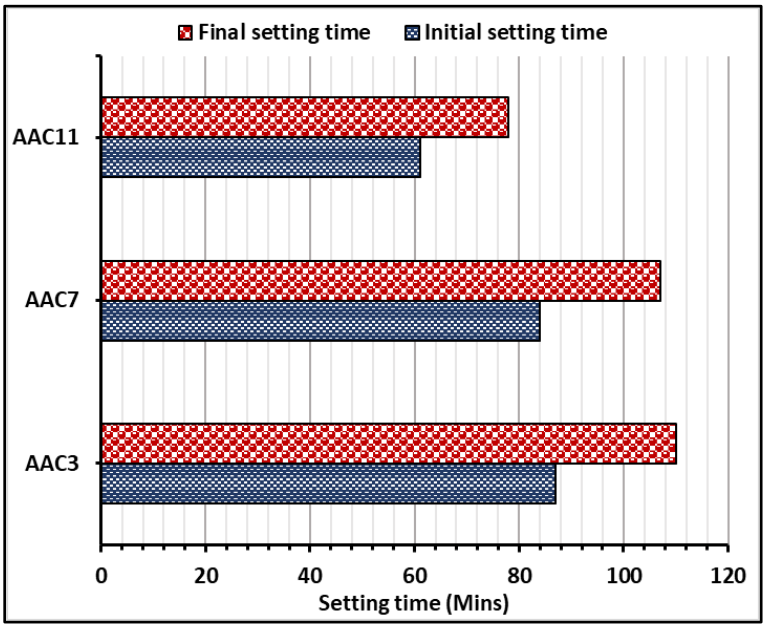

Figure 13 Initial and Final setting times of optimum one-part AAC blends.

3.6 XRD analysis of hydration products

XRD analysis was performed on pastes of samples with the highest strength (AAC3, AAC7 and AAC11) at 28 days and for longer ages (at 90 and 180 days), as presented in Fig. 14. Major hydration products can be identified and are composed chiefly from CaO-Al_2O_3-MgO-SiO_2 compounds. The utilisation of a dry alkaline (CaO) activator, in the mix, transforms the crystallinity diffraction patterns into amorphicity status and leads to the presence of prevailing vitreous phases. The major products phases were specifically tetra calcium aluminate hydrate, CAH (C_4AH_{13}), calcium alumina silicate hydrates, St (stratlingite – C_2ASH_8), and Akermanite, (Ak) ($Ca_2MgSi_2O_7$) [17][66][67][56]. Moreover, Gameiro [67] stated that calcium silicate hydrate (CSH) overlaps with the lime (calcite) peak in these blends, with higher MK (≥ 33% MK). XRD patterns of AAC3 as presented in Fig. 14a. This figure reveals that at the age of 28 days, a slight reduction of the dominant Quartz (SiO_2) crystalline phase that existed in the raw MK at $2\theta = 26^o$.

This slight reduction indicates the remaining large amounts of this crystalline quartz are in a non-reactant status. On the other hand, this reduction was sharp at age of 90 days and even more at age of 180 days, presenting more dissolution of crystalline SiO_2 and transforming into alkaline-silicates strains. This dissolution was induced by the formation of extra Ak products at the longer ages. The fact of reducing crystalline quartz phases and the formation of vitreous Ak, led to the development of significant strength after 90 and 180 days of (AAC3)[63]. Additionally, a glassy phase of alumina-silicate gel (C-A-S-H) can be indicated in the 2θ range of 25°-30° at age of 28 days, however, due to the semi- amorphous nature, this product disappeared at age of 180 days [69,70]. At the same time, the strong presence of St, is noticed as a permanent phase in the matrix. The formulation of St as dominant substance in the three blends, indicating that this product is stable and is verified as the product responsible for the enhancement of mechanical strength [67,71]. Regardless of the slight increment of the Ak mineral peak at 90 and 180 days of AAC7 (in Fig. 14b), crystalline quartz can be noticed in an increment trend from 28 to 180 days. The growth of St peaks can be noticed clearly, through the entire range of diffraction with increment of LKD, causing a higher strength for AAC7. This indicates that the lime (CaO) generated from LKD is causing a significant dissolution of aluminate and silicate species [72], and consumes all alkaline substances resulting no mark of any efflorescence. The high amounts of MgO from NP have strongly contributed to presence of amorphous phases, such as Ak together with the reactive CaO from LKD. This reaction introduced new bonds such as Ca-Mg-Si, which have a high contribution to the strength. C_4AH_{13} (CAH) was present in minor quantities due to the instability of this phase through the curing aging [67]. Additionally, portlandite ($Ca(OH)_2$) peaks were not found extensively due to the modified LKD and MK in the blends, as this peak may appear in low MK blends [67]. A range of reaction products can be noticed similarly in AAC11 as in Fig. 14c, with LKD calcined at 450°C. The amounts of Ak can be observed with less quantities in the all ages of AAC11 with higher amounts calcite (C) than AAC3 and AAC7 that formulated through the ages. This was observed in the strength development for both levels of thermal treatment. However, the diffraction patterns of this blend are presenting growth of crystalline quartz in two major peaks at $2\theta = 26^{o}$ and 47^{o}. This caused a dip in the equivalent of 90- and 180-days strength, for AAC11.

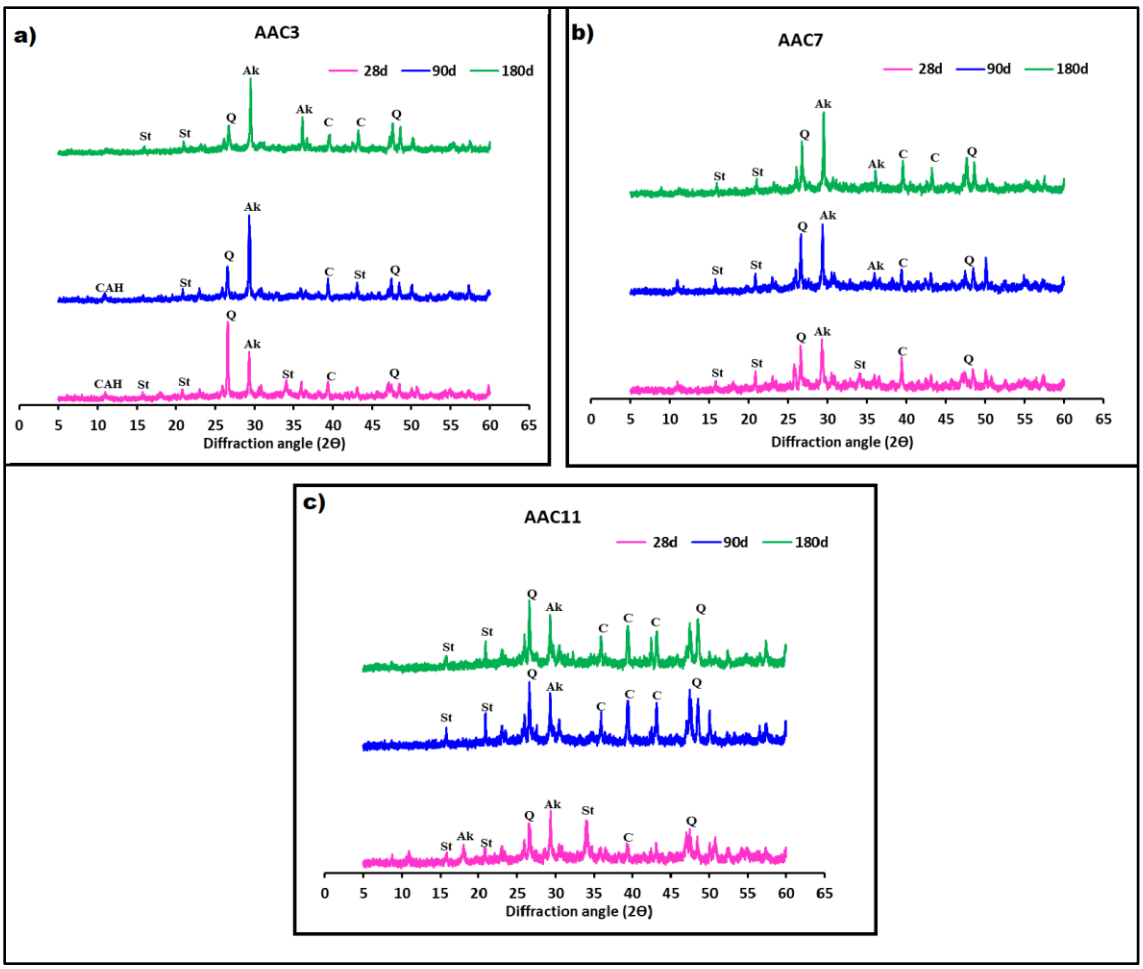

Figure 14. XRD patterns of a) AAC3, b) AAC7, c) AAC11 at 28, 90 and 180 days.

3.7 FTIR analysis of hydration products

The FTIR (Fourier-transform infrared) spectra was reproduced for pastes of AAC3, AAC7 and AAC11 blends, and were investigated after 28,90 and 180 days of curing, as shown in Fig. 15a new absorption bands were recorded at 1642 and 1636 cm^{-1}, for the vibration bending H–O–H in all blends at 90 and 180 days. The appearance of water absorption bands are a clue for the crystalline H_2O of the hydrated products such as C-S-H or C-A-H [73]. In all spectra, the typical carbonate phases C-O band, appeared in the following bands 1406-1418 and 874cm^{-1} was observed. This is similar to infrared in the raw LKD in Fig. 4. However, the intensity of this band was reduced with the right shifting of its location and has become wider at 90 and 180 days for the blends, except for the AAC11 blend, as shown in Fig. 15a-c. This attributed to the calcined LKD at 950 ^oC, has purer and more reactive CaO than 450 ^oC calcination in the case of AAC11, which has more groups of $CaCO_3$. The asymmetric stretching band starting from 1200-900 cm^{-1} region of Si-O and Al-O were noticed in all spectra of the blends. These bands reveal the strong evidence of Aft/AFm phases such as stratlingite (C_2ASH_8) and mono-carboaluminate $Ca_4A_{12}(CO_3)(OH)_{12}$ / $_5H_2O$ [74]. It can be noticed that this band was very wide at 28 days and transformed to be sharp

and narrow at 90 and 180 days with shifting to lower wavenumber in both blends AAC3 and AAC7. It was revealed that such this phenomenon is correlated to the breakdown of covalent bonds of silicate networks, which become less strong and lead to the formation of more non-bridging oxygen (Si–O bonds) that was simply undergone to more condensation and polymerisation [75]. Contrarily, these bands remained unchanged in blend AAC11 for ages of 28, 90 and 180 days. This has led to the development of phases with a non-ordered structure, with a variation of bond length and angles [76], which was in accordance with the reduced strength of AAC11.

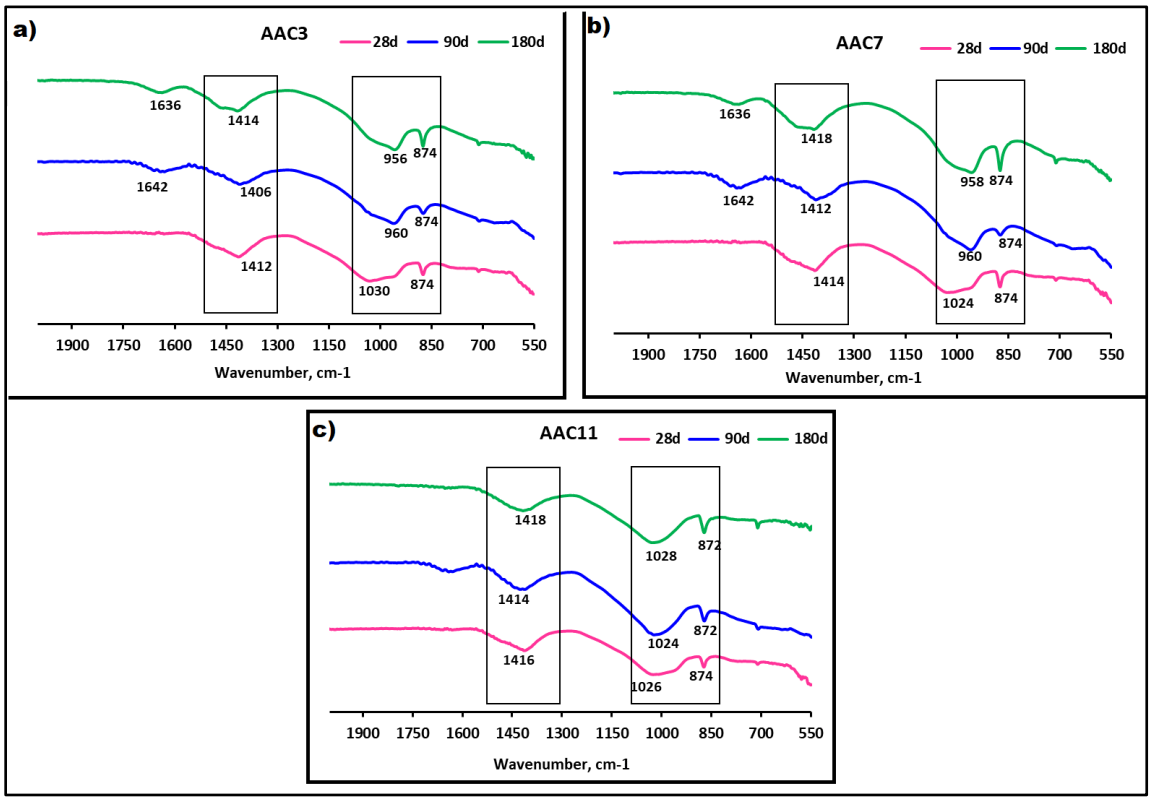

Figure 15. FTIR-spectra of hardened pastes of a) AAC3, b) AAC7, c) AAC11 after 28, 90 and 180days curing.

3.8 SEM analysis of hydrates

The SEM micrographs for AAC3,7 and 11 at 28 days of curing are shown in Fig. 16. The microstructure of hardened pastes shows the significant existence of the un-reactant MK in all blends at 28 days, which can be identified by fine and lamellar particles with random non uniform shapes and similar to particles of raw MK appeared previously in Fig. 3c. However, the un-reactant MK has very limited quantities in blend AAC3, as shown in Fig. 16a, and highest quantities in AAC11, as seen in Fig. 16c. This illustrates the pozzolanic reaction of Si and Al with Ca^{+2} cations, which encourages further dissolution and breaking the Si–O and Al–O bonds in both MK and NP [77]. Ak products can be distinguished clearly as a predominant phase of flat continuous gels in all blends, but its lowest appearance can be seen in AAC11, which agrees with the XRD patterns. The trend of reaction mechanism during the hydration process is with the increment of reactive

calcined LKD at 950 ºC, where there is an increment in the operation of extra dissolution of Al/Si constituents.

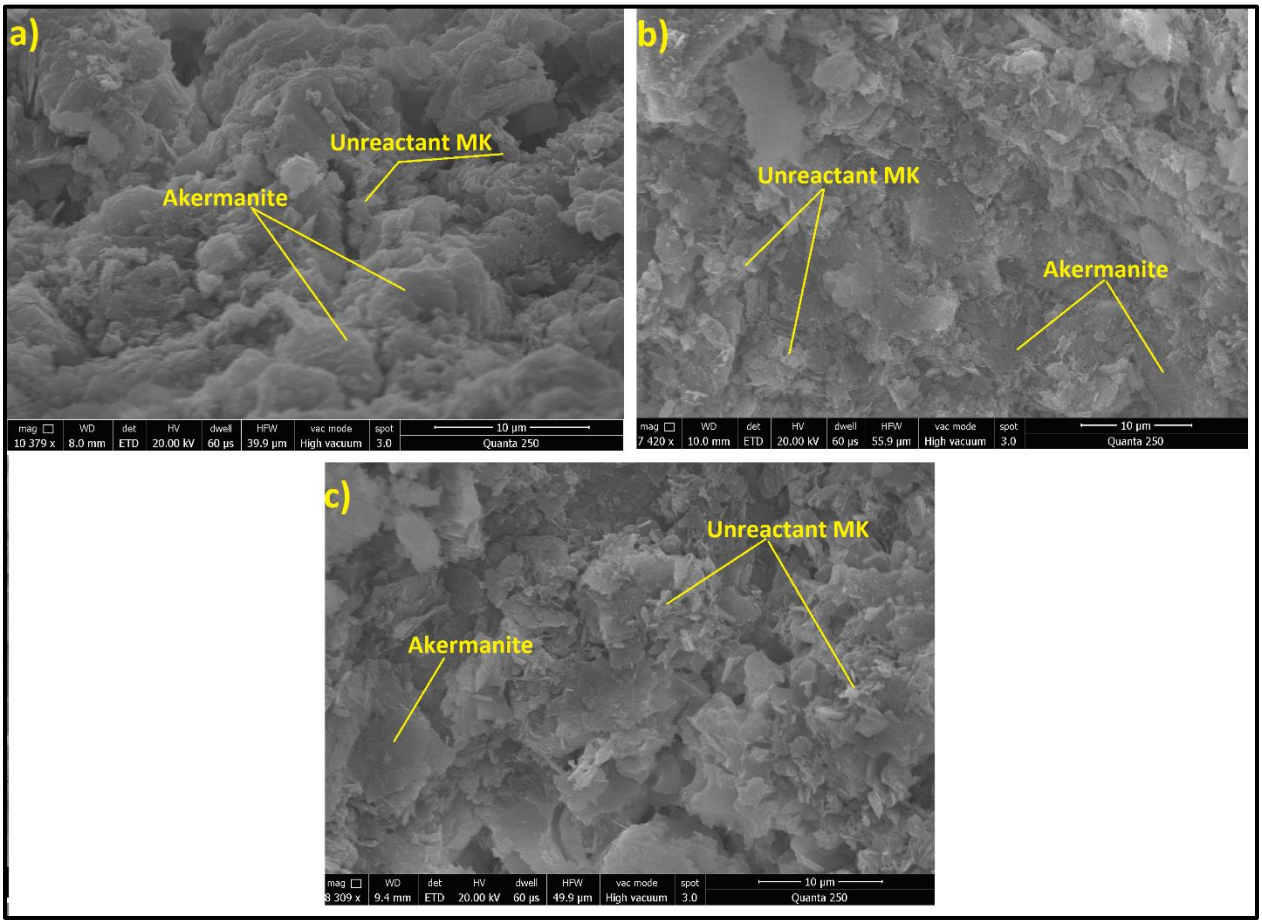

Figure 16. SEM micrographs for a) AAC3, b) AAC7 and c) AAC11 at 28 days

Fig. 17 presents the SEM micrographs of hardened pastes of optimum blends AAC3, 7, 11 at curing age of 90 days. While the matrix of blend AAC7 and AAC11, presented in Fig. 17b and c, is exhibiting un-reactant particles of MK. The amounts of these particles, decreased in blend AAC7 at the age of 90 days compared to 28 days, with the development of more hydrates, such as Ak and St of darker grey tone. On the other hand, it can be significantly recognised from the microstructure of AAC3, as shown in Fig. 17a, that this blend is mostly free any un-reactant particles and showed higher microstructure density. This indicates a large transformation of MK and NP particles into dense gels of hydration products (Ak and St) through long term curing, which in turn resulted in a significant development of strength for the AAC3 blend.

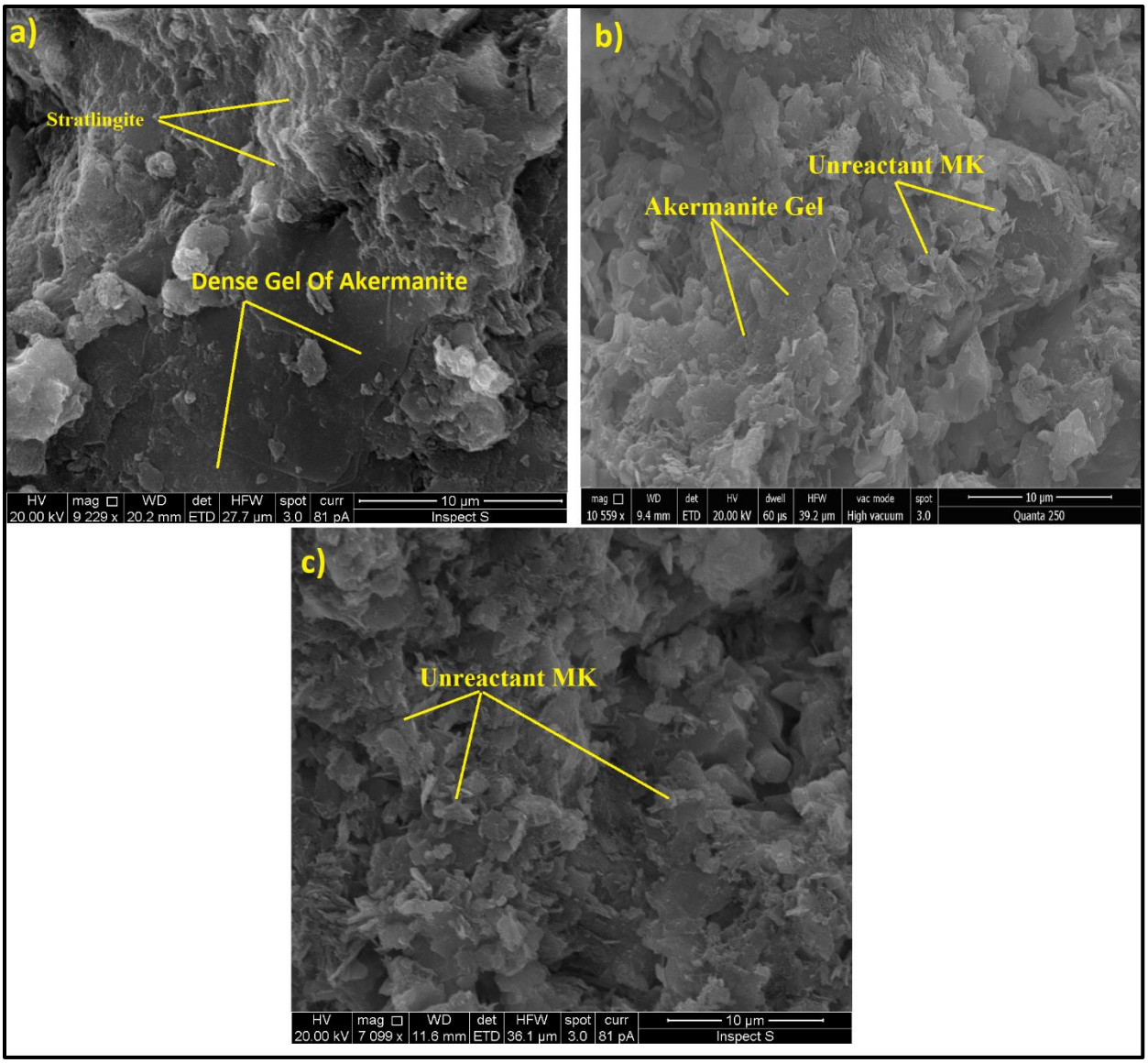

583

584 *Figure 17. SEM micrographs for a) AAC3, b) AAC7 and c) AAC11 at 90 days*

585

586 While it could be clearly noticed that the internal matrix of AAC3 as in Fig. 18a at the age of 180
587 day, has significant increment of the formulation of a dense phase characteristic of cementitious
588 Ak compared to 90 day which strongly reveals the progression of alkali-activation till the age of
589 180 day and the total disappearance of any un-reactant grains. However as shown in Fig. 18b, this
590 dense gel was less presence in AAC7. On the other hand, the microstructure of AAC11 has shown
591 prevalence of un-reactant particles such as MK and very low gels of Ak as shown in Fig. 18c.

592

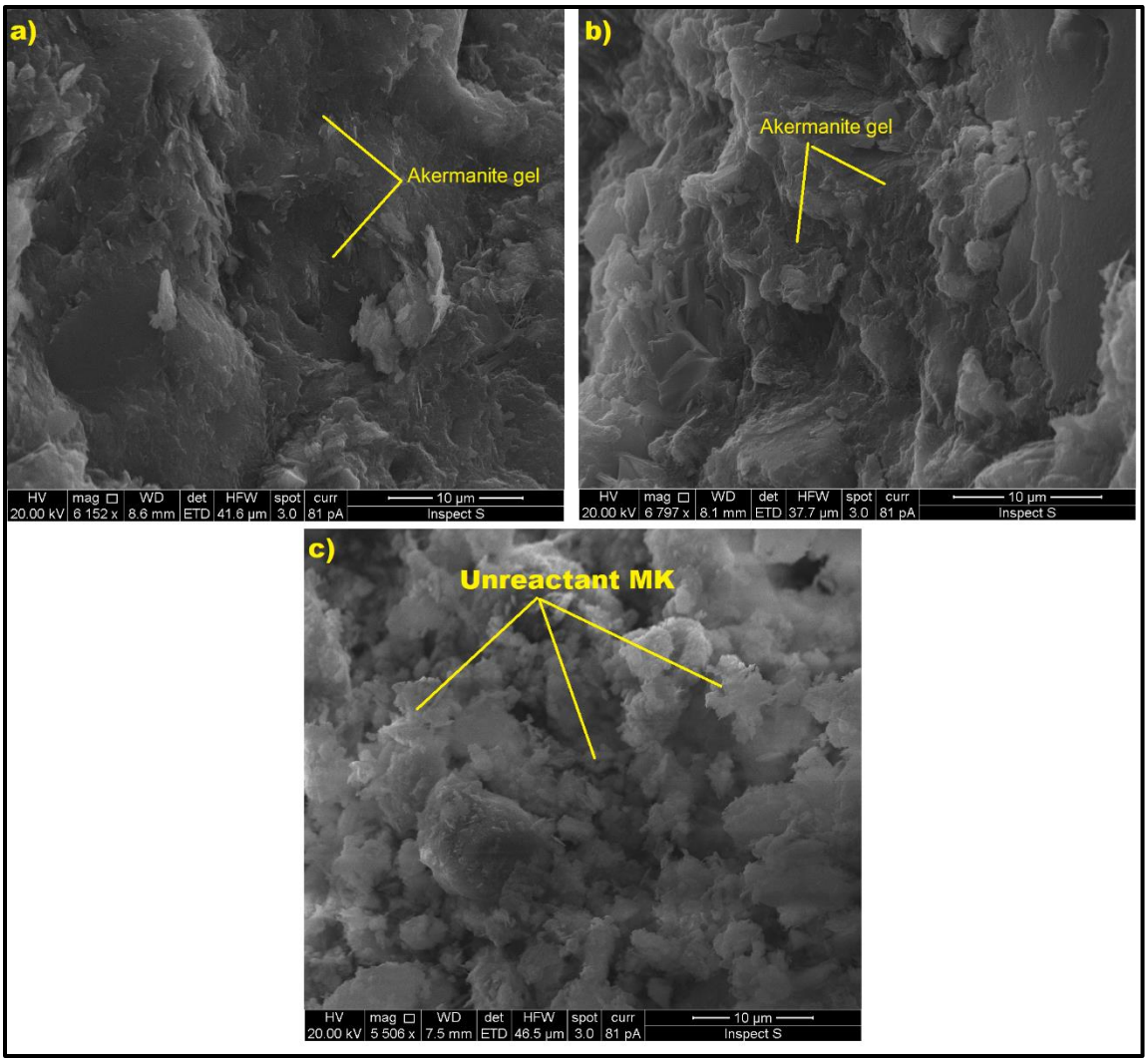

Figure 18 SEM micrographs for a) AAC3, b) AAC7 and c) AAC11 at 180 days

4. Conclusions

Based on the experimental outcomes of using thermally activated Lime Kiln Dust (LKD) that was proposed as solid waste material rich in calcium oxide in the formulation of a second generation one-part AAC cement, the following points can be summarised:

- More than 51% increase in strength after 28 days of curing just for highly reactive calcined LKD at temperature of 950ºC was achieved in the blend containing metakaolin (35 wt.%) and natural pozzolan (30 wt.%).
- Significant increase of rate of strength development after 28 days of curing and continued until 180 days that reached 51 MPa for increased proportion of 950ºC calcined LKD and metakaolin was revealed.

- A high degree of alkali-activation was developing within the synthetic system until 180 days, without showing any marks of efflorescence or presence of unreacted alkaline substances were reported.
- The setting times of the optimised blends were in the acceptable range of setting times in the past studies of one-part AAC and cement types in British standards.
- According to the results of XRD, TG-DTA and FTIR, the thermal treatment at 950°C were evidently participating in breaking the crystalline phases of the original materials and showed strong evidence of transforming to amorphous phases.
- The characterisation findings by XRD, FTIR and SEM, have confirmed that the development of hydration products is responsible for the strength at 28, 90 and 180 days. These products include stratlingite, St (C_2ASH_8) and Akermanite, (Ak) ($Ca_2MgSi_2O_7$).
- The developed one-part AAC has introduced a comparable performance, in regard of the strength, setting times and morphology compositions, to the traditional AAC synthesised from commercial hazardous chemicals. However, there are some limitations, i.e. the durability investigations such as chloride and alkaline attacks which are recommended as a future work.

Acknowledgement

The corresponding author would like to acknowledge the financial support provided by the Iraqi Ministry of Higher Education and Scientific Research and from University of Babylon.

References

[1] U.S. Geological Survey, Mineral commodity summaries 2019, Virginia, 2019. doi:https://doi.org/10.3133/70202434.

[2] C. Shi, A.F. Jiménez, New cements for the 21st century: The pursuit of an alternative to Portland cement, Cem. Concr. Res. 41 (2011) 750–763. doi:10.1016/J.CEMCONRES.2011.03.016.

[3] S. Demie, M.F. Nuruddin, N. Shafiq, Effects of micro-structure characteristics of interfacial transition zone on the compressive strength of self-compacting geopolymer concrete, Constr. Build. Mater. 41 (2013) 91–98.

[4] Mineralproducts.org, Novel cements: low energy, low carbon cements, (2017).

[5] J. Davidovits, Geopolymer cements to minimise carbon-dioxide greenhouse-warming, Ceram. Trans. 37 (1993) 165–182.

[6] J.L. Provis, Alkali-activated materials, Cem. Concr. Res. (2017). doi:https://doi.org/10.1016/j.cemconres.2017.02.009.

[7] J.L. Provis, A. Palomo, C. Shi, Advances in understanding alkali-activated materials, Cem.

642 Concr. Res. 78 (2015). doi:10.1016/j.cemconres.2015.04.013.

643 [8] T. Luukkonen, Z. Abdollahnejad, J. Yliniemi, P. Kinnunen, M. Illikainen, One-part alkali-
644 activated materials: A review, Cem. Concr. Res. 103 (2018) 21–34.

645 [9] J.S.J. Van Deventer, J.L. Provis, P. Duxson, Technical and commercial progress in the
646 adoption of geopolymer cement, Miner. Eng. 29 (2012) 89–104.
647 doi:https://doi.org/10.1016/j.mineng.2011.09.009.

648 [10] M. Torres-Carrasco, F. Puertas, Alkaline activation of different aluminosilicates as an
649 alternative to Portland cement: alkali activated cements or geopolymers, Rev. Ing.
650 Construcción. 32 (2017) 5–12.

651 [11] A.T. Almalkawi, S. Hamadna, P. Soroushian, One-part alkali activated cement based
652 volcanic pumice, Constr. Build. Mater. 152 (2017) 367–374.
653 doi:https://doi.org/10.1016/j.conbuildmat.2017.06.139.

654 [12] F. Matalkah, L. Xu, W. Wu, P. Soroushian, Mechanochemical synthesis of one-part alkali
655 aluminosilicate hydraulic cement, Mater. Struct. 50 (2016) 97. doi:10.1617/s11527-016-
656 0968-4.

657 [13] C.C. Ban, P.W. Ken, M. Ramli, Mechanical and Durability Performance of Novel Self-
658 activating Geopolymer Mortars, Procedia Eng. 171 (2017) 564–571.
659 doi:https://doi.org/10.1016/j.proeng.2017.01.374.

660 [14] J.L. Provis, Introduction and scope, RILEM State-of-the-Art Reports. 13 (2014) 1–9.
661 doi:10.1007/978-94-007-7672-2_1.

662 [15] K. De Weerdt, Geopolymers – State of the art, Blindern, 2011.
663 https://www.sintefbok.no/book/download/1018/vinfopubutgivelsercoincoin_project_repor
664 tscoin_report_no_37nettcoin_no_37pdf.

665 [16] A. Heath, K. Paine, S. Goodhew, M. Ramage, M. Lawrence, The potential for using
666 geopolymer concrete in the UK, Proc. Inst. Civ. Eng. Constr. Mater. 166 (2013) 195–203.

667 [17] M.S. Kim, Y. Jun, C. Lee, J.E. Oh, Use of CaO as an activator for producing a price-
668 competitive non-cement structural binder using ground granulated blast furnace slag, Cem.
669 Concr. Res. 54 (2013) 208–214. doi:https://doi.org/10.1016/j.cemconres.2013.09.011.

670 [18] M. Vaccari, F. Gialdini, C. Collivignarelli, Study of the reuse of treated wastewater on waste
671 container washing vehicles, Waste Manag. 33 (2013) 262–267.

672 [19] C. Li, H. Sun, L. Li, A review: The comparison between alkali-activated slag (Si+ Ca) and
673 metakaolin (Si+ Al) cements, Cem. Concr. Res. 40 (2010) 1341–1349.

674 [20] J. Cabrera, M.F. Rojas, Mechanism of hydration of the metakaolin–lime–water system,
675 Cem. Concr. Res. 31 (2001) 177–182.

676 [21] S. Licht, Process for synthesis of calcium oxide, (2016).
677 http://www.freepatentsonline.com/9297082.html (accessed June 12, 2019).

678 [22] Production of purified calcium carbonate, (1993).
679 https://patents.google.com/patent/EP0558275A1 (accessed June 12, 2019).

680 [23] H.A. Abdel-Gawwad, K.A. Khalil, Application of thermal treatment on cement kiln dust
681 and feldspar to create one-part geopolymer cement, Constr. Build. Mater. 187 (2018) 231–

237. doi:https://doi.org/10.1016/j.conbuildmat.2018.07.161.

[24] Y. Wang, X. Liu, W. Zhang, Z. Li, Y. Zhang, Y. Li, Y. Ren, Effects of Si/Al ratio on the efflorescence and properties of fly ash based geopolymer, J. Clean. Prod. (2019) 118852. doi:10.1016/J.JCLEPRO.2019.118852.

[25] H.A. Abdel-Gawwad, S.R.V. García, H.S. Hassan, Thermal activation of air cooled slag to create one-part alkali activated cement, Ceram. Int. 44 (2018) 14935–14939. doi:https://doi.org/10.1016/j.ceramint.2018.05.089.

[26] M.M. Miller, R.M. Callaghan, Lime Kiln Dust as a Potential Raw Material in Portland Cement Manufacturing, (2004). http://www.cement.org/basics/ (accessed May 14, 2019).

[27] J.L. Provis, S.A. Bernal, Geopolymers and related alkali-activated materials, Annu. Rev. Mater. Res. 44 (2014) 299–327.

[28] P. Nath, P.K. Sarker, Use of OPC to improve setting and early strength properties of low calcium fly ash geopolymer concrete cured at room temperature, Cem. Concr. Compos. 55 (2015) 205–214.

[29] British Standard Institution, 196-6: 2010, BSI Standards Limited, London, n.d.

[30] A.M. Rashad, A.A. Hassan, S.R. Zeedan, An investigation on alkali-activated Egyptian metakaolin pastes blended with quartz powder subjected to elevated temperatures, Appl. Clay Sci. 132–133 (2016) 366–376. doi:https://doi.org/10.1016/j.clay.2016.07.002.

[31] British Standard Institution, 196-3: 2016, 2016.

[32] British Standard Institution, 196-1: 2016, BSI Standards Limited, London, 2016.

[33] J.O. Hill, R.K. Verma, Thermal Analysis | Coupled Techniques☆, in: P. Worsfold, C. Poole, A. Townshend, M.B.T.-E. of A.S. (Third E. Miró (Eds.), Academic Press, Oxford, 2019: pp. 6–11. doi:https://doi.org/10.1016/B978-0-12-409547-2.14484-1.

[34] C. Vizcayno, R.M. De Gutierrez, R. Castello, E. Rodriguez, C.E. Guerrero, Pozzolan obtained by mechanochemical and thermal treatments of kaolin, Appl. Clay Sci. 49 (2010) 405–413.

[35] P.S. Nayak, B.K. Singh, Instrumental characterization of clay by XRF, XRD and FTIR, Bull. Mater. Sci. 30 (2007) 235–238.

[36] G. Kakali, T. Perraki, S. Tsivilis, E. Badogiannis, Thermal treatment of kaolin: the effect of mineralogy on the pozzolanic activity, Appl. Clay Sci. 20 (2001) 73–80. doi:https://doi.org/10.1016/S0169-1317(01)00040-0.

[37] G.-R. Miguel, H. Juan, B. Leticia, N.-M. Joaquín, R.-G.M. E., Characterization of Calcium Carbonate, Calcium Oxide, and Calcium Hydroxide as Starting Point to the Improvement of Lime for Their Use in Construction, J. Mater. Civ. Eng. 21 (2009) 694–698. doi:10.1061/(ASCE)0899-1561(2009)21:11(694).

[38] B.R. Ilić, A.A. Mitrović, L.R. Miličić, Thermal treatment of kaolin clay to obtain metakaolin, Hem. Ind. 64 (2010) 351–356.

[39] H.M. Owaid, R. Hamid, M.R. Taha, Influence of thermally activated alum sludge ash on the engineering properties of multiple-blended binders concretes, Constr. Build. Mater. 61

(2014) 216–229. doi:https://doi.org/10.1016/j.conbuildmat.2014.03.014.

[40] H. Justnes, I. Meland, J.O. Bjoergum, J. Krane, T. Skjetne, Nuclear magnetic resonance (NMR)—a powerful tool in cement and concrete research, Adv. Cem. Res. 3 (1990) 105–110.

[41] T. Kovářík, P. Bělský, P. Novotný, J. Říha, J. Savková, R. Medlín, D. Rieger, P. Holba, Structural and physical changes of re-calcined metakaolin regarding its reactivity, Constr. Build. Mater. 80 (2015) 98–104. doi:https://doi.org/10.1016/j.conbuildmat.2014.12.062.

[42] A. Ghorbel, M. Fourati, J. Bouaziz, Microstructural evolution and phase transformation of different sintered Kaolins powder compacts, Mater. Chem. Phys. 112 (2008) 876–885. doi:https://doi.org/10.1016/j.matchemphys.2008.06.047.

[43] J. Šesták, B. Foller, Some aspects of composite inorganic polysialates, J. Therm. Anal. Calorim. 108 (2012) 511–517.

[44] A. Arulrajah, A. Mohammadinia, A. D'Amico, S. Horpibulsuk, Effect of lime kiln dust as an alternative binder in the stabilization of construction and demolition materials, Constr. Build. Mater. 152 (2017) 999–1007. doi:https://doi.org/10.1016/j.conbuildmat.2017.07.070.

[45] C.A. Strydom, Q.I. Roode, J.H. Potgieter, Thermogravimetric and X-ray powder diffraction analysis of precipitator dust from a rotating lime kiln, Cem. Concr. Res. 26 (1996) 1269–1276. doi:https://doi.org/10.1016/0008-8846(96)00096-8.

[46] M. Vafaei, A. Allahverdi, Influence of calcium aluminate cement on geopolymerization of natural pozzolan, Constr. Build. Mater. 114 (2016) 290–296. doi:https://doi.org/10.1016/j.conbuildmat.2016.03.204.

[47] R. Firdous, D. Stephan, J.N.Y. Djobo, Natural pozzolan based geopolymers: A review on mechanical, microstructural and durability characteristics, Constr. Build. Mater. 190 (2018) 1251–1263. doi:https://doi.org/10.1016/j.conbuildmat.2018.09.191.

[48] D. Bondar, C.J. Lynsdale, N.B. Milestone, N. Hassani, A.A. Ramezanianpour, Effect of heat treatment on reactivity-strength of alkali-activated natural pozzolans, Constr. Build. Mater. 25 (2011) 4065–4071. doi:https://doi.org/10.1016/j.conbuildmat.2011.04.044.

[49] M.X. Peng, Z.H. Wang, Q.G. Xiao, F. Song, W. Xie, L.C. Yu, H.W. Huang, S.J. Yi, Effects of alkali on one-part alkali-activated cement synthesized by calcining bentonite with dolomite and Na2CO3, Appl. Clay Sci. 139 (2017) 64–71. doi:10.1016/j.clay.2017.01.020.

[50] J. Davidovits, Geopolymers based on natural and synthetic metakaolin-A critical review, Adv. Ceram. Compos. 38 (2017) 201.

[51] M. Kimata, N. Nishida, M. Shimizu, S. Saito, T. Matsui, Y. Arakawa, Anorthite megacrysts from island arc basalts, Oceanogr. Lit. Rev. 1 (1996) 50.

[52] S. Chithra, G. Dhinakaran, Effect of hot water curing and hot air oven curing on admixed concrete, Int. J. ChemTech Res. CODEN IJCRGG. (2014) 1516–1523.

[53] D.S. Perera, O. Uchida, E.R. Vance, K.S. Finnie, Influence of curing schedule on the integrity of geopolymers, J. Mater. Sci. 42 (2007) 3099–3106.

[54] B. Singh, G. Ishwarya, M. Gupta, S.K. Bhattacharyya, Geopolymer concrete: A review of

761 some recent developments, Constr. Build. Mater. 85 (2015) 78–90.

762 [55] D. Feng, J.L. Provis, J.S.J. van Deventer, Thermal Activation of Albite for the Synthesis of
763 One-Part Mix Geopolymers, J. Am. Ceram. Soc. 95 (2012) 565–572. doi:10.1111/j.1551-
764 2916.2011.04925.x.

765 [56] C. Ferone, B. Liguori, I. Capasso, F. Colangelo, R. Cioffi, E. Cappelletto, R. Di Maggio,
766 Thermally treated clay sediments as geopolymer source material, Appl. Clay Sci. 107
767 (2015) 195–204. doi:https://doi.org/10.1016/j.clay.2015.01.027.

768 [57] B.K. Shahraki, B. Mehrabi, K. Gholizadeh, M. Mohammadinasab, Thermal behavior of
769 calcite as an expansive agent, J. Min. Metall. B Metall. 47 (2011) 89–97.

770 [58] P. Duxson, G.C. Lukey, J.S.J. van Deventer, Physical evolution of Na-geopolymer derived
771 from metakaolin up to 1000 C, J. Mater. Sci. 42 (2007) 3044–3054.

772 [59] P. He, D. Jia, M. Wang, Y. Zhou, Effect of cesium substitution on the thermal evolution
773 and ceramics formation of potassium-based geopolymer, Ceram. Int. 36 (2010) 2395–2400.

774 [60] X. Guo, H. Shi, L. Chen, W.A. Dick, Alkali-activated complex binders from class C fly ash
775 and Ca-containing admixtures, J. Hazard. Mater. 173 (2010) 480–486.
776 doi:https://doi.org/10.1016/j.jhazmat.2009.08.110.

777 [61] S. Ahmari, L. Zhang, Utilization of cement kiln dust (CKD) to enhance mine tailings-based
778 geopolymer bricks, Constr. Build. Mater. 40 (2013) 1002–1011.
779 doi:https://doi.org/10.1016/j.conbuildmat.2012.11.069.

780 [62] H. Madani, A.A. Ramezanianpour, M. Shahbazinia, E. Ahmadi, Geopolymer bricks made
781 from less active waste materials, Constr. Build. Mater. 247 (2020) 118441.
782 doi:https://doi.org/10.1016/j.conbuildmat.2020.118441.

783 [63] S. Yaseri, V. Masoomi Verki, M. Mahdikhani, Utilization of high volume cement kiln dust
784 and rice husk ash in the production of sustainable geopolymer, J. Clean. Prod. 230 (2019)
785 592–602. doi:10.1016/J.JCLEPRO.2019.05.056.

786 [64] British Standard Institution, 197-1: 2011, BSI Standards Limited, London, 2011.

787 [65] T. Luukkonen, Z. Abdollahnejad, K. Ohenoja, P. Kinnunen, M. Illikainen, Suitability of
788 commercial superplasticizers for one-part alkali-activated blast-furnace slag mortar, J.
789 Sustain. Cem. Mater. 8 (2019) 244–257. doi:10.1080/21650373.2019.1625827.

790 [66] A. Gameiro, A. Santos Silva, P. Faria, J. Grilo, T. Branco, R. Veiga, A. Velosa, Physical
791 and chemical assessment of lime–metakaolin mortars: Influence of binder:aggregate ratio,
792 Cem. Concr. Compos. 45 (2014) 264–271.
793 doi:https://doi.org/10.1016/j.cemconcomp.2013.06.010.

794 [67] A. Gameiro, A. Santos Silva, R. Veiga, A. Velosa, Hydration products of lime–metakaolin
795 pastes at ambient temperature with ageing, Thermochim. Acta. 535 (2012) 36–41.
796 doi:https://doi.org/10.1016/j.tca.2012.02.013.

797 [68] A. Gameiroa, A.S. Silvab, R. Veigac, A. Velosad, Metakaolin-Lime Hydration Products
798 and Phase Stability: A Microscopy Analysis, B. Ext. (2011) 31.

799 [69] A. Elimbi, H.K. Tchakoute, M. Kondoh, J.D. Manga, Thermal behavior and characteristics
800 of fired geopolymers produced from local Cameroonian metakaolin, Ceram. Int. 40 (2014)

4515–4520.

[70] J.I. Escalante-García, A.F. Fuentes, A. Gorokhovsky, P.E. Fraire-Luna, G. Mendoza-Suarez, Hydration Products and Reactivity of Blast-Furnace Slag Activated by Various Alkalis, J. Am. Ceram. Soc. 86 (2003) 2148–2153.

[71] A. Bakolas, E. Aggelakopoulou, A. Moropoulou, S. Anagnostopoulou, Evaluationof pozzolanic activity and physicomechanical characteristics in metakaolin-limepastes, J. Therm. Anal. Calorim. 84 (2006) 157–163. doi:10.1007/s10973-005-7262-y.

[72] M.S. Morsy, Y.A. Al-Salloum, T.H. Almusallam, H. Abbas, Mechanical properties, phase composition and microstructure of activated Metakaolin-slaked lime binder, KSCE J. Civ. Eng. 21 (2017) 863–871.

[73] J.L. Provis, J.S.J. Van Deventer, Geopolymers: structures, processing, properties and industrial applications, Elsevier, 2009.

[74] M. Horgnies, J.J. Chen, C. Bouillon, Overview about the use of Fourier Transform Infrared spectroscopy to study cementitious materials, WIT Trans. Eng. Sci. 77 (2013) 1743–3533. doi:10.2495/MC130221.

[75] J.N.Y. Djobo, A. Elimbi, H.K. Tchakouté, S. Kumar, Mechanical activation of volcanic ash for geopolymer synthesis: effect on reaction kinetics, gel characteristics, physical and mechanical properties, RSC Adv. 6 (2016) 39106–39117.

[76] W. Mozgawa, J. Deja, Spectroscopic studies of alkaline activated slag geopolymers, J. Mol. Struct. 924 (2009) 434–441.

[77] C. Medina, I.F. Sáez del Bosque, E. Asensio, M. Frías, M.I. Sánchez de Rojas, Mineralogy and microstructure of hydrated phases during the pozzolanic reaction in the sanitary ware waste/Ca (OH) 2 system, J. Am. Ceram. Soc. 99 (2016) 340–348.